Dynamic Bending Rigidity of a 200-bp DNA in 4 mM Ionic Strength: A Transient Polarization Grating Study

Alexei N. Naimushin, Bryant S. Fujimoto, and J. Michael Schurr
Department of Chemistry, University of Washington, Seattle, Washington 98195-1700 USA

ABSTRACT DNA may exhibit three different kinds of bends: 1) permanent bends; 2) slowly relaxing bends due to fluctuations in a prevailing equilibrium between differently curved secondary conformations; and 3) rapidly relaxing dynamic bends within a single potential-of-mean-force basin. The dynamic bending rigidity (κ_d), or equivalently the dynamic persistence length, $P_d = \kappa_d/k_BT$, governs the rapidly relaxing bends, which are responsible for the flexural dynamics of DNA on a short time scale, $t \leq 10^{-5}$ s. However, all three kinds of bends contribute to the total equilibrium persistence length, P_{tot}, according to $1/P_{tot} \cong 1/P_{pb} + 1/P_{sr} + 1/P_d$, where P_{pb} is the contribution of the permanent bends and P_{sr} is the contribution of the slowly relaxing bends. Both P_d and P_{tot} are determined for the same 200-bp DNA in 4 mM ionic strength by measuring its optical anisotropy, $r(t)$, from 0 to 10 μs. Time-resolved fluorescence polarization anisotropy (FPA) measurements yield $r(t)$ for DNA/ethidium complexes (1 dye/200 bp) from 0 to 120 ns. A new transient polarization grating (TPG) experiment provides $r(t)$ for DNA/methylene blue complexes (1 dye/100 bp) over a much longer time span, from 20 ns to 10 μs. Accurate data in the very tail of the decay enable a model-independent determination of the relaxation time (τ_R) of the end-over-end tumbling motion, from which $P_{tot} = 500$ Å is estimated. The FPA data are used to obtain the best-fit pairs of P_d and torsion elastic constant (α) values that fit those data equally well, and which are used to eliminate α as an independent variable. When the relevant theory is fitted to the entire TPG signal ($S(t)$), the end-over-end rotational diffusion coefficient is fixed at its measured value and α is eliminated in favor of P_d. Neither a true minimum in chi-squared nor a satisfactory fit could be obtained for P_d anywhere in the range 500–5000 Å, unless an adjustable amplitude of azimuthal wobble of the methylene blue was admitted. In that case, a well-defined global minimum and a reasonably good fit emerged at $P_d = 2000$ Å and $\langle \delta\zeta^2 \rangle^{1/2} = 25°$. The discrimination against P_d values <1600 Å is very great. By combining the values, $P_{tot} = 500$ Å and $P_d = 2000$ Å with a literature estimate, $P_{pb} = 1370$ Å, a value $P_{sr} = 1300$ Å is estimated for the contribution of slowly relaxing bends. This value is analyzed in terms of a simple model in which the DNA is divided up into domains containing m bp, each of which experiences an all-or-none equilibrium between a straight and a uniformly curved conformation. With an appropriate estimate of the average bend angle per basepair of the curved conformation, a lower bound estimate, $m = 55$ bp, is obtained for the domain size of the coherently bent state. Previous measurements suggest that this coherent bend is not directional, or phase-locked, to the azimuthal orientation of the filament.

INTRODUCTION

It has been suggested that DNA exhibits three different kinds of bends, namely 1) permanent bends, 2) slowly relaxing bends due to fluctuations in a prevailing equilibrium between differently curved secondary conformations, and 3) rapidly relaxing bends within a single potential-of-mean-force basin (Song and Schurr, 1990; Schurr et al., 1992; 1997a,b). Although all three types of bends contribute to determine the total persistence length (Schurr et al., 1997a; Trifonov et al., 1987; Harrington, 1993), only the last contributes to the *dynamics* of DNA flexure on short time scales, $t \lesssim 10^{-5}$ *s. The value of the total persistence length*, $P_{tot} = 500$ Å, is reasonably well known from a variety of measurements, at least under standard conditions. However, much less is known about the separate contributions of the different kinds of bends.

Permanent bends

Intrinsic curvature of certain sequences is well-established, and is directional in the sense that the bend is phase-locked (to some degree) to the azimuthal orientation of the filament (Trifonov et al., 1987; Harrington, 1993). However, the magnitude of that intrinsic curvature may reflect a tilted equilibrium between intrinsically bent and intrinsically straight(er) states (Nelson et al., 1987), because it varies to some extent with sequence context (Dlakic and Harrington, 1996, 1998), and depends strongly on various environmental factors, such as temperature (Diekmann, 1987; Chan et al., 1990), concentration of alcohols (Sprous et al., 1995), and concentration of Mg^{2+} ions (Brukner et al., 1994; Dlakic and Harrington, 1995), all of which can be varied to completely remove the curvature of certain sequences. The apparent absence of any effect of permanent bends on single-molecule force versus extension curves at moderate to high extension, including the very precise data recently reported (Wang et al., 1997), suggests that moderate tension, far below that required for 30% extension, may also shift the secondary structure equilibrium in favor of intrinsically straight states. Estimating the contribution of directional permanent bends to the total persistence length is a

Received for publication 30 July 1999 and in final form 3 December 1999.
Address reprint requests to Dr. J. Michael Schurr, Dept. of Chemistry, University of Washington, Campus Box 351700, Seattle, WA 98195-1700. Tel.: 206-543-6681; Fax: 206-685-8665; E-mail: schurr@chem.washington.edu.

0006-3495/00/03/1498/21 $2.00

delicate matter that requires sequence averaging of the permanent bends and ensemble averaging of the nonpermanent bends and twists, and the results in general depend upon both the anisotropy and noncentrosymmetry of the bending potential, which govern the coupling between twisting and bending (Schurr, 1985; Schurr et al., 1995; Allison and Schurr, 1997). The total persistence lengths for particular sequences were simulated by using Trifonov's wedge model (Bolshoy et al., 1991) for the directional permanent bends and the simplest possible isotropic Hookean twisting and bending potentials (Schellman and Harvey, 1995). These were found to obey an approximate relation, which was later generalized to give

$$1/P_{tot} \cong 1/P_{pb} + 1/P_{sr} + 1/P_{d}, \quad (1)$$

where $P_{pb} = 1370$ Å is the contribution of the permanent bends, P_{sr} is the contribution of slowly relaxing bends due to conformational fluctuations, and P_d is the contribution of rapid dynamic bends (Schurr et al., 1997a,b). Because the available experimental data rule out all extant nearest-neighbor permanent bending models (Dlakic and Harrington, 1996, 1998), including the Trifonov wedge model, the particular value obtained for P_{pb} must be regarded as somewhat tentative.

Dynamic bends

The dynamic persistence length, P_d, is related to the dynamic bending rigidity (A_d) that governs the short-time ($t \lesssim 1$ μs) flexural dynamics of DNA by

$$P_d \equiv A_d/k_B T \quad (2)$$

where k_B is Boltzmann's constant and T the absolute temperature. Experimental estimates of P_d have come from analyses of the decays of the transient photoinduced dichroism (TPD) (Allison et al., 1989), and transient electric birefringence (TEB) (Eden and Sunshine, 1989), and dichroism (TED) (Diekmann et al., 1982; Pörschke et al., 1987), and more recently from EPR spin-label spectra (Hustedt et al., 1993; Okonogi et al., 1999).

The TPD data for a 209-bp DNA were compared with Brownian dynamics simulations of the optical anisotropies of intrinsically straight model filaments with selected values of P_d and the torsion elastic constant (α) (Allison et al., 1989). It was concluded that the data could *not* be satisfactorily fitted by $P_d = 500$ Å. Among the trial values considered, the best fit was obtained *over the span of the presented data* by $P_d = 1000$ Å and $\alpha = 7.6 \times 10^{-12}$ dyne cm. However, the assumption that $P_{tot} = P_d$ very likely yielded a lower best-fit P_d value than would have been obtained, had the effect of any permanent and/or slowly relaxing bends to diminish P_{tot} and the end-over-end tumbling time (τ_R) been taken into account. The contribution of flexural *dynamics* to the fluorescence polarization anisotropy (FPA) or TPD is governed entirely by P_d, whereas the rate of end-over-end tumbling reflects P_{tot}, which is generally smaller than P_d. Thus, setting $P_d = P_{tot}$ is expected to yield a compromise best-fit value that underestimates P_d. An approximate analytical theory for treating weakly bending rods allows for separate adjustment of the end-over-end tumbling time and the P_d that governs the flexural dynamics (Song et al., 1990). Unfortunately, the TPD data for the 209-bp restriction fragment at 5°C extend only to 2×10^{-6} s, which is less than one-third of the expected τ_R value, so the quality of the fit at any longer times in the very tail of the decay curve could not be assessed, and τ_R could not be reliably extracted in an independent manner by fitting that tail. An equally good, if not superior, fit of the model to the data could almost certainly be obtained by using a somewhat smaller α, a somewhat larger $P_d > 1000$ Å, and a longest tumbling time corresponding to $P_{tot} \simeq 500$ Å $< P_d$. It is crucial to obtain precise optical anisotropy data extending much farther into the tail of the curve so that the τ_R can be obtained separately from the best-fit P_d. A much more extensive least-squares fitting of the model to the experimental data to determine the statistically "allowed" range of P_d values would also be desirable, but that is impractical to implement via Brownian dynamics. The approximate analytical theory for treating weakly bending rods and circles has been tested against Brownian dynamics simulations (Song et al., 1990; Heath et al., 1995, 1996b) and found to work well, even in the presence of regular directional permanent bends (Allison and Schurr, 1997), and provides a means to rapidly calculate χ^2 at very many points of a grid search to map out the allowed range of P_d, as described below.

Extracting a value of P_d from TED and TEB decay curves is complicated by several factors. Unlike the FPA and TPD, which measure known *self*-correlation functions, the TED and TEB off-field decays monitor *mutual* correlation functions of a kind that depends on the mechanism of orientation of the DNA in the electric field, which is not known with certainty (Allison and Nambi, 1992). This uncertainty is especially acute in regard to the nonlinear part of the response of the DNA to the electric field, which may be important, because nonlinear effects are evident in the experimental data. For example, the shape of the decay curve, in particular the relative amplitude of the fast initial transient, increases substantially (up to 20-fold) with electric field strength from 1 to 20 kV/cm for DNAs containing 95–250 bp (Eden and Sunshine, 1989; Diekmann et al., 1982; Pörschke, 1987). In addition, overshoot of the birefringence after the electric pulse is shut off is observed for DNAs as short as 300 bp, even at rather low electric field strengths (1 kV/cm) (Eden and Sunshine, 1989). These findings suggest that bending strain energy is stored in some of the DNA molecules during the pulse. Any distortion of the molecule or alteration of its response function must arise from a nonlinear effect. According to the theory developed

for purely linear excitation mechanisms, the relative contribution of the collective bending modes to the decay of the relevant *mutual* correlation functions is much smaller than in the case of the corresponding *self*-correlation functions, and the amplitude associated with the longest bending relaxation time is negligibly small (Heath et al., 1995). These somewhat surprising effects are due to extensive cancellation of terms in the particular *mutual* correlation functions that are expected for *linear* orientation by induced dipole, correlated induced dipole, permanent dipole, and saturated induced dipole mechanisms. The limited available theoretical information about *nonlinear* effects comes from simulations of charged DNA-like rods with a bend-dependent orientation mechanism that more plausibly represents the effects of ion-atmosphere polarization than any of those noted above (Elvingson, 1992). The results indicate that filaments, which are initially oriented perpendicular to the electric field pulse, acquire a substantial horseshoe bend as they undergo electrophoresis toward the closed end of the horseshoe. This is tantamount to a very substantial enhancement of the initial amplitude of the longest bending mode. Of course, the bending will be asymmetrical when initiated at any position other than the center, and the longer arm is expected to be more aligned with the field than the shorter. Relaxation of an asymmetrically bent DNA after the electric field is turned off almost certainly proceeds by realigning the short arm on one side of the bend with the longer arm on the other. This would be expected to produce an increase in magnitude of the birefringence, which is a likely explanation for the overshoot during the off-field decays of the DNAs with $N \geq 300$ bp. In any case, when the off-field TED and TEB decays for DNAs with $N = 120–250$ bp are fitted to a double-exponential function, and the relaxation time of the fast initial transient is *assumed* to correspond to the longest bending normal mode, the optimum agreement between predicted and observed values is obtained for $P_d = 2100$ Å (Song and Schurr, 1990). This value is fairly precisely determined by the data. However, until it can be unequivocally established that *nonlinear* bending of transversely oriented DNAs during the pulse actually does sufficiently enhance the amplitude of the longest bending mode, the validity of this P_d value is open to question. In fact, if the orientation mechanism is assumed to be exclusively linear, a much smaller value, $P_d = 500$ Å, can account well for the relaxation times of the fast initial transients, which are then dominated by higher bending modes. However, the predicted relative amplitudes of the fast initial transients are invariant to electric field strength, contrary to observation (Allison and Nambi, 1992). If such a low value of P_d is ruled out by other experiments that admit a range of values containing 2100 Å, then the validity of such a high value becomes less doubtful, and it may provide a relatively precise guide to the actual value under the prevailing 2 mM ionic strength conditions.

We have been exploring an alternative approach, in which the FPA of ethidium intercalated in 13 synthetic duplexes of different composition and length (12(3), 24(2), 36(3), 48(3), 60(1), and 72(1) bp), in two native restriction fragments containing 43 and 69 bp, and in several long native DNAs was measured and analyzed (Fujimoto et al., 1993, 1994b). The objective is to fit all of these data with a common value of α and P_d, and eventually to assess the increase of the effective hydrodynamic cylinder radius (due to permanent bends) from $R_H = 10.1 \pm 0.2$ Å for $N = 12$ and 24 bp up to an expected plateau value at large $N \geq 200$ bp. According to Brownian dynamics simulations of 72-bp model DNAs with and without regular permanent bends (15.6° every 24.5 Å), the effect of the permanent bends is to increase the effective R_H for azimuthal spinning by only 3%, from 10.0 to 10.3 Å (Allison and Schurr, 1997). If the increase in R_H from 12 to 72 bp is *assumed* to be $\leq$1.04-fold, then the FPA data imply that $P_d \geq 1500$ Å for all 10 DNAs with $N = 36–72$ bp. This work is still ongoing and a full discussion will be presented elsewhere.

The EPR spin-label experiments (Hustedt et al., 1993; Okonogi et al., 1999) differ in several important regards from the FPA and TPD experiments discussed above. 1) The principal axes of the hyperfine tensors of the spin-labels make a relatively small angle (~15–20°) with respect to the helix-axis, so the EPR spectrum is much more sensitive to end-over-end tumbling and bending than to azimuthal spinning and twisting motions. In contrast, in the FPA and TPD experiments the transition dipole makes a much larger angle (70–75°) with respect to the helix-axis, so those experiments are relatively more sensitive to azimuthal spinning and twisting than to tumbling and bending motions. 2) The primary effect of the bending motions of sufficiently short DNAs on the EPR spectrum is a rapid pre-averaging of the elements of the hyperfine tensor. In such a case, the data reflect simply the equilibrium mean-squared amplitudes of the dynamic bending motions, which do not depend on the hydrodynamic radius. 3) The label is covalently attached to a particular base in the sequence, rather than distributed along the DNA, as are the intercalated dyes used in the TPD and FPA experiments. By changing the position of the spin-label in the DNA, the relative sensitivity of the EPR spectrum to bending modes of even and odd symmetry can be varied. In fact, the variations of the observed mean-squared amplitudes of internal angular motion of such spin-labels with the length of homologous DNA (12, 24, 36, 48, and 96–100 bp) and with the relative position of the label in the DNA are in excellent accord with the analytical theory (Okonogi et al., 1999). The original experiments on one kind of sequence with a particular spin-label yielded $P_d = 2400$ Å (Hustedt et al., 1993). More recent experiments on a different kind of DNA sequence with a new spin-label yield $P_d = 1500–1700$ Å (Okonogi et al., 1999). These results pertain to 0.1 M ionic strength, and are almost certainly the most reliable estimates presently available for

such standard conditions. Independent assessment of P_{tot} for these same DNAs cannot be made in these EPR experiments.

Slowly relaxing bends associated with a fluctuating conformation equilibrium

A great deal of evidence for slowly relaxing conformational equilibria in both linear and circular DNAs has been reported previously by our and other laboratories, and was just recently reviewed (Schurr et al., 1997a). NMR evidence for slowly relaxing conformational exchanges at certain sites in small duplexes has also been reported (Kennedy et al., 1993; McAteer et al., 1995; McAteer et al., submitted for publication; Gaudin et al., 1995, 1997; Paquet et al., 1996; Spielmann, 1998). However, the evidence that the involved conformations exhibit different intrinsic curvatures is less abundant and more indirect. A prevailing equilibrium between a nearly straight secondary structure and one or more intrinsically curved (or superhelical) conformations would necessarily contribute both to the average extent of permanent bending and to slowly relaxing fluctuations about that. As noted previously, the sensitivity of sequence-dependent permanent bends to various environmental factors is consistent with a prevailing equilibrium between two or more states with different intrinsic curvature. The appearance of long-lived structural isomers of multimers of a 147-bp intrinsically curved DNA in electrophoretic gels is also consistent with a slowly relaxing equilibrium between differently curved secondary conformations (N. C. Stellwagen, personal communication).

If slowly relaxing fluctuations between alternative conformations with different intrinsic curvature contribute significantly to the mean-squared amplitude of bending of the DNA (away from its average curved conformation), then it follows that an imposed bending strain must shift that conformational equilibrium, and thereby change those properties that are sensitive to average secondary structure, such as the torsion elastic constant, the intrinsic binding affinity for ethidium, and the circular dichroism (CD) spectrum. Such an experiment was performed by circularizing a 181-bp DNA, and profound changes in those same properties were actually observed (Heath et al., 1996a). In fact, the available data from our and other laboratories suggest that, as the bending strain is increased by decreasing the size of the DNA circle, a structural transition occurs between 360 and 250 bp (cf. Fig. 1) (Shore and Baldwin, 1983; Clendenning and Schurr, 1994; Horowitz and Wang, 1984; Shimada and Yamakawa, 1985; Taylor and Hagerman, 1990). Moreover, this transition may well be cooperative. Because the average bend per basepair required to induce the structural transition ($\theta_1 \leq 1.5°$) is much smaller than the root-mean-squared (RMS) bend between basepairs of an unstrained DNA ($\sim$6–7°), one may infer that coherence of the bend over many basepairs is more important than the absolute magnitude of the bend for stabilizing the curved state.

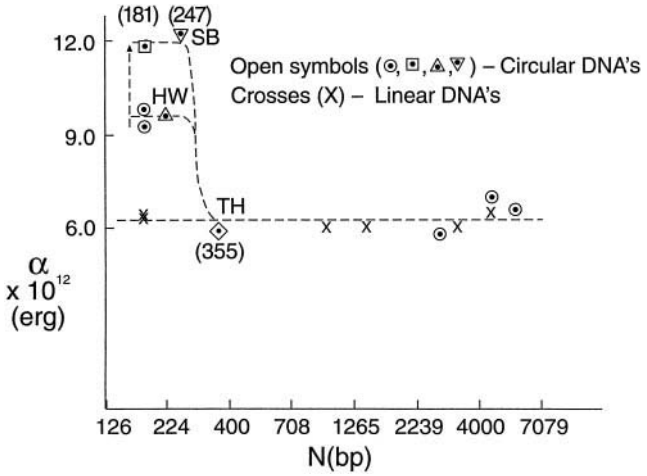

FIGURE 1 Torsion elastic constant α versus DNA length (N) for various DNAs. The crosses are linear DNAs and the open symbols are circular DNAs. SB denotes the data of Shore and Baldwin (1983) as analyzed by Clendenning and Schurr (1994). HW denotes the data of Horowitz and Wang (1984) as analyzed by Shimada and Yamakawa (1985) and Frank-Kamenetskii et al. (1985). TH denotes the data of Taylor and Hagerman (1990). The open circles and square denote the data of Heath et al. (1996a).

These observations suggest that the average domain size of the prevailing curved conformer might be considerably larger than a single basepair. Because a modest degree of coherent bending strain suffices to shift the prevailing secondary structure equilibrium toward the more curved state, fluctuations in that equilibrium are expected to contribute to the equilibrium RMS curvature and $1/P_{tot}$ of the unstrained DNA.

A bend-dependent conformational equilibrium might play a significant role in the activation of transcription. A number of transcriptional activators bind at specific sites in the proximal promoter region, 50–250 bp upstream from the RNA polymerase binding site, and induce large bends in the DNA either directly at their binding sites (Schultz et al., 1991; Passner and Steitz, 1997; Kim et al., 1994; Grosschedl et al., 1994; Rice et al., 1996; Sjottem et al., 1997; Geiselmann, 1997; Perez-Martin and de Lorenzo, 1997; Diebold et al., 1998; Engelhorn and Geiselmann, 1998; Davis et al., 1999; Parkhurst et al., 1996, 1999) or indirectly via DNA looping (Mossing and Record, 1986; Gralla, 1991, 1996; Schleif, 1992; Rippe et al., 1995). The activation of transcription by DNA looping was formerly ascribed to an increase in concentration of the activator (bound to one end of the loop) in the vicinity of the RNA polymerase binding site (at the other end of the loop), which was postulated to facilitate activation by protein-protein interactions (Mossing and Record, 1986; Rippe et al., 1995). Now that the bending strain in small loops with $N \leq 250$ bp is known to alter their secondary structure, one could equally well postulate that protein-induced DNA bending, either direct or via DNA looping, induces an allosteric transition of the DNA to an

alternative secondary structure that somehow facilitates the binding or kinetics of transcription initiation by the RNA polymerase. CAP and Sp1 are transcriptional activators that induce large contact bends, ~90° (Kolb et al., 1983; Wu and Crothers, 1984; Liu-Johnson et al., 1986; Passner and Steitz, 1997) and 60° (Sjottem et al., 1997; Ikeda et al., 1993), at their respective binding sites. Evidence that both specific CAP binding to supercoiled plasmids and specific Sp1 binding to a 1074-bp linear DNA induce long-range alterations of the DNA secondary structure was recently discussed (Schurr et al., 1997a).

Goals and strategy

Our primary goal is to assess the dynamic bending rigidity of DNA via time-resolved optical emission and absorption anisotropy experiments. Specifically, we measure the FPA of intercalated ethidium in a 200-bp DNA at high time resolution (~40 ps) from 0 to 120 ns, and the transient photoinduced dichroism of intercalated methylene blue in the same DNA at lower time resolution (10 ns) from 0 to 10 μs by means of a new transient polarization grating (TPG) method (Naimushin et al., 1999b), which is an alternative to direct TPD experiment (Hogan et al., 1982, 1983; Allison et al., 1989). By detecting the photoinduced dichroism diffractively with a *single* detector, the TPG experiment completely eliminates certain systematic errors and faithfully monitors the loss of dichroism out to sufficiently long times that the τ_R can be reliably determined by fitting just the very tail of the TPG data (Naimushin et al., 1999a,b). The best-fit τ_R value of our most dilute sample is analyzed to give $P_{tot} \cong$ 500 Å for this 200-bp DNA in the prevailing 4 mM ionic strength. This best-fit τ_R value is used in the subsequent analysis of both FPA and TPG data. The FPA data are analyzed to determine the empirical relation between the best-fit α- and P_d values that fit the FPA data equally well. This empirical relation is then used to eliminate α as an adjustable parameter in the subsequent fitting of the TPG data to determine the best-fit value of P_d, which is found to be 2000 (−200, +300) in 4 mM ionic strength at 21°C.

Our secondary objective is to estimate the contribution, $1/P_{sr}$, of slowly relaxing bends to $1/P_{tot}$ by using the best available estimates of P_{tot}, P_{pb}, and P_d in Eq. 1. To rationalize the estimated $P_{sr} = 1300$ Å, we adopt a very simple model, in which the DNA is divided into average domain sizes of m basepairs, each of which exhibits an all-or-none equilibrium between a straight and a uniformly curved conformation. By assuming an intrinsic bend, $\theta_1 = 1.46°$/bp, for the latter in accord with Fig. 1, we estimate a lower bound for the average domain size, $m \geq 55$ bp.

MODEL AND ANISOTROPY THEORY

The DNA is modeled by a chain of N identical rigid subunits, each of which is connected to its neighbors on either side by Hookean torsion and bending springs (Schurr et al., 1992). These springs represent the *dynamic* torsional and bending rigidities, respectively. On the time scale of our experiment ($t \leq 10^{-5}$ s), each molecule exhibits 1) a *common* intrinsic curvature due to permanent bends, which contains an average contribution from the prevailing equilibrium between intrinsically straight and curved conformations, plus 2) a *variable* "intrinsic" curvature due to fluctuations in that same equilibrium, which are effectively frozen on the time scale of our experiment. As a consequence of its intrinsic curvature, the average end-to-end distance and τ_R of each molecule will be significantly smaller than reckoned simply according its P_d. Moreover, because every molecule may have a slightly different intrinsic curvature (due to slowly relaxing bends) that is *not* averaged out by dynamic flexure on the time scale of the end-over-end rotation, it may be necessary to consider a *distribution* of mean end-to-end distances (Schurr and Fujimoto, submitted for publication) and end-over-end tumbling times, as will be done below. The effect of the dynamic bending rigidity is to resist the deformation of any molecule from its particular intrinsically curved state of mechanical equilibrium. The total intrinsic curvature is assumed to be sufficiently modest that the dynamics of bending, twisting, and uniform azimuthal spinning of the vast majority of molecules are practically identical to each other and to that reckoned for an intrinsically straight rod, albeit one with an enhanced effective cylinder radius to account for the increased friction of azimuthal spinning of the bent filament (Schurr et al., 1997b; Allison and Schurr, 1997). The validity of this assumption was demonstrated by Brownian dynamics simulations of 72-bp model DNAs with regular permanent bends (Allison and Schurr, 1997).

We adopt the analytical theory developed for deformable filaments with mean local cylindrical symmetry, in which case the optical anisotropy is given by Schurr et al. (1992), Schurr (1984), and Schurr and Fujimoto (1988),

$$r(t) = \frac{I_{\parallel}(t) - I_{\perp}(t)}{I_{\parallel}(t) + 2I_{\perp}(t)} = (\mathrm{ARF})(2/5) \sum_{n=0}^{2} I_n(\infty) C_n(t) F_n(t) \qquad (3)$$

For the FPA, $I_{\parallel}(t)$ and $I_{\perp}(t)$ are the fluorescence intensities with polarizations parallel and perpendicular, respectively, to that of an infinitely short exciting pulse. In the case of TPD, $I_{\parallel}(t)$ and $I_{\perp}(t)$ are replaced by $\Delta A_{\parallel}(t) = A_{\parallel}(t) - A_{\parallel}^{o}$ and $\Delta A_{\perp}(t) = \Delta A_{\perp}(t) - A_{\perp}^{o}$, respectively, where $A_{\parallel}(t)$ and $A_{\perp}(t)$ are the absorbances for probe beams with polarizations parallel and perpendicular, respectively, to that of the photobleaching pulse, and $A_{\parallel}^{o} = A_{\perp}^{o}$ pertains to the unperturbed solution prior to arrival of the photobleaching pulse. The maximum initial anisotropy is 2/5,

$$\mathrm{ARF} = \langle P_2(\cos\beta)\rangle^2 \cong 1 - 6\sigma^2 \qquad (4)$$

is the amplitude reduction factor due to rapid unresolved *isotropic* wobble of the dye relative to the DNA, and σ^2 is

the mean-squared amplitude of *small* isotropic dye wobble. For the FPA of intercalated ethidium, ARF = 0.90 and $\sigma \cong 7°$ (Schurr et al., 1992), and for the FPA of methylene blue (MeBl), ARF = 0.73 and $\sigma \cong 12°$ (Fujimoto et al., 1994a). However, for the TPD of intercalated MeBl, Austin and co-workers often reported considerably lower ARF values, in some cases as low as 0.40 (Hogan et al., 1982, 1983; Allison et al., 1989), and this anomaly was more pronounced for GC-rich DNAs. The evidence that such low initial anisotropies of DNA/methylene blue complexes in TPD experiments stem primarily from enhanced azimuthal wobble is discussed in the Data Analysis section. The $I_n(\infty)$ are internal correlation functions *after* the rapid relaxation of both isotropic and excess (beyond isotropic) azimuthal dye wobble (Schurr et al., 1992; Schurr, 1984; Schurr and Fujimoto, 1988),

$$I_0(\infty) = [(3/2)\cos^2\varepsilon - 1/2]^2 \tag{5a}$$

$$I_1(\infty) = 3\cos^2\varepsilon \sin^2\varepsilon \exp(-\langle\delta\zeta^2\rangle) \tag{5b}$$

$$I_2(\infty) = (3/4)\sin^4\varepsilon \exp(-4\langle\delta\zeta^2\rangle) \tag{5c}$$

where ε is the polar angle between the transition dipole of the dye and the local symmetry axis of the DNA, and $\langle\delta\zeta^2\rangle$ is the *excess* mean-squared amplitude of *azimuthal* dye wobble. The dye wobble manifested in the FPA of either ethidium or MeBl is believed to be small in amplitude and *isotropic*, so we take $\langle\delta\zeta^2\rangle = 0$ in those cases. However, for the TPG of DNA/MeBl complexes, $\langle\delta\zeta^2\rangle$ will be entered as an adjustable parameter into the fitting protocol. The $C_n(t)$ are twisting correlation functions (Schurr, 1984; Schurr et al., 1992; Heath et al., 1996b)

$$C_n(t) = (1/N)\sum_{m=1}^{N} \exp\left[-\left((n^2 k_B T t/N\gamma) + n^2 \sum_{l=2}^{N} d_l^2\, Q_{ml}^2 (1 - e^{-t/\tau_l})\right)\right] \tag{6}$$

where N is the number of basepairs, γ is the friction factor per basepair for azimuthal rotation around the local symmetry axis, and d_l^2, Q_{ml}, and τ_l are the mean-squared amplitude, projection onto the mth basepair, and relaxation time, respectively, of the lth normal torsion mode. Expressions for the latter quantities are given elsewhere (Schurr, 1984; Schurr et al., 1992; Heath et al., 1996b; Allison and Schurr, 1979). The d_l^2, Q_{ml}, τ_l, and $C_n(t)$ are readily calculated when N, α, R_H, T, and the solvent viscosity η are specified. The $F_n(t)$ are tumbling correlation functions for the weakly bending rod model (Song et al., 1990; Heath et al., 1996b)

$$F_n(t) = (1/N')\sum_{m=1}^{N'} \exp\left[-(6 - n^2)\left(D_R t + (b/P_d)\sum_{l=3}^{N'} (S_{m+1,l} - S_{m,l})^2 (1 - e^{-t/T_l})\right)\right] \tag{7}$$

where N' is the number of subunits, b = 31.8 nm is the length (diameter) of the contiguous spherical subunits of this weakly bending rod model, and S_{ml} and T_l are the projection onto the mth subunit and relaxation time of the lth bending normal mode, respectively. Formulas and numerical methods to calculate S_{ml} and T_l from the dynamical matrix are described elsewhere (Schurr et al., 1992; Song et al., 1990; Heath et al., 1996b). The dynamical matrix depends only upon N'. The rotational diffusion coefficient for end-over-end tumbling (D_R) is here regarded as an adjustable parameter to be determined separately by fitting the tail of the TPG data. The $F_n(t)$ are readily calculated when N', b, D_R, P_d, T, and η are specified.

$C_0(t) = 1.0$ does not relax at all, whereas $C_1(t)$ and $C_2(t)$ relax much more rapidly than $F_0(t)$, because uniform spinning of a 200-bp DNA is much faster than end-over-end tumbling. Consequently, the $n = 0$ term in Eq. 3 dominates at long times, and for sufficiently long times that the bending modes have all relaxed (i.e., $t > T_3$), the anisotropy decay becomes a single exponential with relaxation time $\tau_R = 1/(6D_R)$.

The rapid wobble of intercalated ethidium relaxes in ~50 ps (Schurr et al., 1992), whereas that of intercalated MeBl (in its FPA) relaxes in ~200 ps (Fujimoto et al., 1994a). Negligible error is incurred by assuming that such motions are infinitely rapid compared to the collective twisting and bending motions. Equations 6 and 7 for $C_n(t)$ and $F_n(t)$ were derived by assuming that no cross terms couple twisting and bending on the potential surface, and that any geometrical coupling between such motions is also negligible. In that case, the twisting and bending motions are separable, and linear Langevin equations apply in the molecular frame in each case (Schurr et al., 1992; Song et al., 1990; Heath et al., 1996b; Allison and Schurr, 1979). The effect of hydrodynamic interactions on the twisting dynamics was earlier shown to be negligible (Allison, 1983). Hydrodynamic interactions were incorporated into the Langevin equations for the bending dynamics, as described previously (Song et al., 1990). The 31.8 Å diameter of the contiguous spherical subunits is chosen to yield diffusion coefficients for uniform rotation and translation that agree with the predictions of Tirado and Garcia de la Torre (1979, 1980) for rigid cylinders with R_H = 12.5 Å, which in turn agree with measurements on short restriction fragments (Elias and Eden, 1981). The elementary subunit used in the calculation of $C_n(t)$ is one basepair and its hydrodynamic cylinder radius is taken

to be 12 Å. This value, which significantly exceeds 10.1 Å, is intended to account for enhanced friction of azimuthal spinning of a 200-bp molecule when it exhibits intrinsic curvature. Evidence that the effective R_H for diffusional spinning reaches a plateau value that might be ~12 Å for $N \geq 170$ bp was discussed previously (Schurr et al., 1997b). In any case, the bending and end-over-end tumbling motions are very insensitive to the choice of R_H.

Although Eqs. 3, 6, and 7 take full account of *torques* arising from the torsion potential and *forces* arising from the bending potential, they take no account of the *forces* arising from the torsion potential. Such forces stem from a geometrical coupling between twisting and bending, and generally vanish unless the molecule is simultaneously both bent and twisted (Heath et al., 1996b). It was demonstrated via Brownian dynamics simulations that these *forces* arising from the torsion potential have no significant effect on the $r(t)$ of a 196-bp model DNA along an equilibrium trajectory (Heath et al., 1996b), although they have a very substantial effect on the rate of conversion of excess twist into writhe in a small circular DNA (Chirico and Langowski, 1994). Equilibrium $r(t)$ curves for 196-bp model DNAs, which were simulated by incorporating all forces and torques, could be successfully fitted and analyzed by using Eqs. 3–7 (Heath et al., 1996b). This remained true even when regular permanent bends were incorporated into the Brownian dynamics simulations of a 72-bp model DNA provided that D_R was adjusted separately and R_H was allowed to increase slightly to account for the enhanced friction of uniform azimuthal spinning (Allison and Schurr, 1997). Although the analytical theory embodied in Eqs. 3–7 has been well tested against Brownian dynamics simulations, the aforementioned tests do not extend to times $t > 200$ ns.

Finally, we note that the model of a weakly bending rod that is used to analyze the data is valid only for DNA lengths (L) such that $L \lesssim (0.6)\ P_d$ (Song et al., 1990; Fujimoto and Schurr, submitted for publication). It is advantageous to work with the longest possible DNA subject to this constraint so the amplitude of the longest bending mode is as large as possible. Because of the prevailing uncertainty regarding P_d we elected to study a 200-bp DNA, although one could certainly go as high as 250 bp if $P_d \geq$ 1500 Å, as appears to be the case.

Fixed parameters in the model

$C_n(t)$ is calculated for $N = 200$ subunits (1 subunit/bp), $T =$ 294 K, $\eta = 0.009779$ poise, $R_H = 12.0$ Å, $h = 3.4$ Å, and $\gamma = 4\pi R_H^2\ h\ \eta = 6.02 \times 10^{-23}$ dyne cm s. All sums are evaluated numerically. $F_n(t)$ is calculated for $N' = 21$ contiguous subunits with 31.8 Å diameter, using the same values of T, η. D_R is taken to be the measured value, except when a distribution of D_R is considered. In that case, an $F_n(t)$ curve is calculated for each subcomponent (j) of the population using its appropriate value of D_{Rj}, which is estimated by a scaling procedure described in the Data Analysis section, and the resulting $(F_n(t))_j$ curves are then averaged.

Pertinent times

Because of the very wide span of times accessed in this study, it is pertinent to consider the relaxation times of some of the most relevant motions. The 50- and 200-ps relaxation times for the wobbles of excited ethidium and MeBl, respectively, in their intercalation sites have already been mentioned. The relaxation time of the longest torsion normal mode is $\tau_2 \cong [4\eta\pi R_H^2\ h/(4\alpha \sin^2(\pi/2N))] \cong 40.7$ ns for $\alpha = 6.0 \times 10^{-12}$ dyne cm and the parameters given above (Schurr et al., 1992; Schurr, 1984; Allison and Schurr, 1979). The relaxation time for the uniform mode of azimuthal spinning in $C_1(t)$ is $\tau_{11} = 4\eta\pi R_H^2\ h \cdot (200)/k_B T =$ 297 ns for the same choice of parameters. This is the longest relaxation time in $C_1(t)$. The relaxation time for the uniform mode of azimuthal spinning in $C_2(t)$ is $\tau_{21} = \tau_{11}/4 = 74$ ns. This is the longest relaxation time in $C_2(t)$. If $P_d = 2000$ Å, the longest bending relaxation time for a 200-bp DNA is $T_2 \cong 325$ ns for the same choice of parameters. More than half of the mean-squared amplitude of angular motion due to bending is associated with this longest bending normal mode. The relaxation time for end-over-end tumbling is found experimentally to be 4.26 μs or 3.80 μs, depending on the DNA concentration. From these times one may infer that the $n = 2$ and 1 terms in Eq. 3 are greatly attenuated by $2\tau_{21} = 148$ ns and $2\tau_{11} = 594$ ns. Beyond $2\tau_{11} = 594$ ns, the $n = 0$ term in Eq. 3 begins to dominate.

MATERIALS AND METHODS

The DNA sample

The 200-bp DNA sample was prepared by copying the sequence from position 233 to 432 of pBR322 by polymerase chain reaction (PCR). This was done using an ExpandTM Long Template PCR System kit from Boehringer Mannheim. This 200-bp DNA contains the entire sequence of the 181-bp DNA (positions 236–417 of pBR322), whose response to imposed bending strain was studied previously by Heath et al. (1996b), and is 56% GC. Details of the sample preparation, purification, and characterization are presented elsewhere (Naimushin, 1999). The purification protocol includes 1) protein digestion with proteinase K and removal of the products by multiple extractions with buffered phenol; 2) exhaustive dialysis alternately versus high salt (HSTE) (500 mM NaCl, 10 mM Tris, 1 mM Na_2 EDTA, pH 8.5 at 21°C) and normal salt (NSTE) (100 mM NaCl, 10 mM Tris, 1 mM EDTA, pH 8.5 at 21°C) buffers at 4°C, terminating finally in the latter; and 3) hydroxyapatite chromatography. The sample characterization includes 1) confirmation of the sequence by direct sequencing; and 2) gel electrophoretic comparison with standards of known length to certify that the tertiary structure is normal with no significant gel retardation (e.g., due to large permanent bends). For the FPA and TPG studies the samples contain 1.5 g/l DNA (i.e., 1.13×10^{-5} M DNA molecules or 2.3 mM basepairs). The buffer contains 5 mM Tris (but no NaCl or Na_2 EDTA) at pH 7.5, and its ionic strength is 4 mM. Although higher ionic strengths were studied up to 47 mM, uncertainties regarding the nature of the MeBl binding at the higher ionic strengths preclude a full

analysis of those data at the present time. DNA concentrations were determined from the UV spectrum of an appropriately diluted sample by assuming $A_{260} \cong 1.0$ for a 0.05 g/l solution. The samples also contain 1 added MeBl per 100 bp for the TPG studies, and 1 added ethidium per 200 bp for the FPA studies. The MeBl was purified as described by Bergmann and O'Konski (1963).

Behavior of methylene blue

The binding constant of MeBl for a single intercalation site at 20°C in 4 mM ionic strength was estimated from the data of Hagmar et al. (1992) in the manner described earlier (Fujimoto et al., 1994a), and found to be $1.9 \times 10^5\ M^{-1}$. Under the prevailing conditions in our 4 mM sample, the MeBl is practically (99.8%) all bound. However, as shown previously, even under low ionic strength conditions, MeBl occupies (at least) three different intercalation sites with very similar unwinding angles (Fujimoto et al., 1994a) and absorption spectra (Hagmar et al., 1992), but very different fluorescence lifetimes (25, 130, and 620 ps). The transient photobleaching of the MeBl (due to triplet formation) was found to arise primarily from the longest-lived of these intercalated species, which was associated with AT, TA, or AA steps (Fujimoto et al., 1994a). These long-lived sites should account for most of the photobleaching in the present TPG experiments. For calf thymus DNA in 8 mM ionic strength, such sites comprise only ~20% of the total bound dye. Nevertheless, from the measured fluorescence lifetimes and relative fluorescence amplitudes, we estimate that the longest-lived sites are responsible for ~75% of the total photobleach under 8 mM (or lower) ionic strength conditions.

At higher ionic strengths the situation is considerably more complex, for the following reason. With increasing ionic strength, not only do the relative populations of the different intercalation sites shift, but the longest-lived fluorescent component, which still dominates the photobleaching, moves from an intercalated site to an outside bound site (Fujimoto et al., 1994a). The latter site exhibits a somewhat shorter fluorescence lifetime (430 ps) and a much greater amplitude of rapid local angular motion, or wobble, which reduces its anisotropy to ~24% of its initial value with a relaxation time of ~100 ps. In contrast, at the lowest ionic strength examined previously (8.3 mM), rapid dye wobble relaxes the FPA of the longest-lived component only modestly to 73% of its starting value with a relaxation time of ~200 ps. In fact, the observed residual anisotropy after relaxation by rapid dye wobble declines progressively with increasing ionic strength from (0.73)(2/5) at 8.3 mM to (0.24)(2/5) at 207 mM (Fujimoto et al., 1994a). Because neither the equilibrium orientation (i.e., ε) nor the distribution of excursion angles of this outside bound dye is known, it is not possible to interpret the *full* anisotropy decay at any but the two very lowest ionic strengths in the present work (4 and 8 mM), for which the experimental decay curves are almost identical. Here we focus solely on the 4 mM ionic strength data. We note that the equilibrium orientation and distribution of excursion angles of MeBl strongly affect the *amplitude*, but not the *rate constant*, of the terminal exponential decay of $r(t)$ due to end-over-end tumbling. Consequently, it is possible to determine τ_R as a function of ionic strength to assess the effects of intermolecular electrostatic interactions on self-rotational diffusion, and the results of that study are discussed elsewhere (Naimushin et al., 1999a). Intermolecular interactions cause almost no change in τ_R as the ionic strength is lowered from 47 to 20 mM, but effect a 12% increase in τ_R upon further lowering to 4 mM. This increase in τ_R is removed simply by a twofold reduction of the DNA concentration. Any effects of intermolecular interactions on the dynamics of internal motions, such as bending, are expected to be much less than on τ_R, and therefore negligible.

Sample protocol

The samples prepared for TPG studies are deoxygenated by bubbling argon saturated with buffer vapor through the solutions for 12–18 h before each experiment. The argon is also blown gently across the top of each sample during the experiments.

The sample cuvette is 1 mm thick by 1 cm in breadth by 4 cm deep. To ameliorate any effects of transient heating and permanent photobleaching, the 300 μl sample volume was stirred by periodically slowly withdrawing and reinjecting a small portion of the sample. This was accomplished using a semi-collapsible tube that was immersed in the sample at one end, and the other contains an upstream N_2 bubble that is alternately pinched and released by a peristaltic pump.

Fluorescence polarization anisotropy measurements

The apparatus and experimental protocols for FPA measurements on the 200-bp DNA/ethidium complexes are reviewed elsewhere (Schurr et al., 1992). However, the atypically high DNA concentration (1.5 g/l), the buffer (5 or 10 mM Tris with no EDTA or NaCl), pH (7.5), and the temperature (294 K) are peculiar to the present experiments. For these measurements the instrumental width of the apparatus was ~40 ps. The analyses of both the FPA and TPD data are discussed in the Data Analysis section.

Transient polarization grating measurements

A detailed description of the TPG instrument is provided elsewhere (Naimushin, 1999; Naimushin et al., 1999b), so only a brief account will be given here. The grating is written in the sample by intersecting two coherent (0.04 cm^{-1} bandwidth) pulses (5 ns) of horizontally propagating laser light (690 nm), which have *orthogonal* (vertical and horizontal) polarizations. Each beam is ~2 mm in diameter and makes an angle $\theta/2 = 20°$ with respect to the grating normal. As a consequence of this excitation, the sample is uniformly bleached by ~1%. This is the fraction of MeBl molecules that undergo intersystem crossing to their triplet states, from which they return to the ground state with a relatively long lifetime of ~10–20 μs in these deoxygenated solutions. The repetition rate of this experiment is 10 s^{-1}. Although the intensity of the superimposed excitation pulses is uniform throughout the grating, the *polarization* of the light varies periodically along the grating from right circular to linear (polarized at $+\pi/4$ from vertical) to left circular to linear (polarized at $-\pi/4$ from vertical), and then back to right circular to begin another period. The regions of the sample that experience circular polarization undergo isotropic (unpolarized) photobleaching in the plane of the grating, whereas those that experience linear polarization undergo anisotropic photobleaching. That is, in the linear polarization regions, those intercalated MeBl molecules with transition dipoles aligned along the local polarization of the light are preferentially excited and become proportionately trapped in their triplet states. Because the MeBl triplet absorbance is negligible in the spectral region of the $S_0 \rightarrow S_1$ absorption band, those molecules are effectively bleached for the duration of their lifetime in the triplet state. In these experiments the triplet state serves merely as a temporary reservoir for optically silent molecules. Due to the anisotropic photobleaching-induced in the zones of linear polarization, the sample becomes uniaxially dichroic in those regions with symmetry axes alternately at $+\pi/4$ and $-\pi/4$ from vertical, as one moves along the grating. The excitation pulse energy (~0.2 mJ) is adjusted so that a MeBl molecule with its transition dipole aligned along the local polarization in a linearly polarized region is cycled through its $S_0 \rightarrow S_1$ transition ~10 times during the pulse, when it fails to reach its triplet state. Consequently, a majority of the photobleached molecules were excited previously during the *same* pulse. A noteworthy feature of the polarization grating is that the uniform intensity creates *no* ordinary thermal phase grating, which would relax by thermal diffusion on the microsecond time scale of interest and potentially complicate the data analysis.

The amplitude of the photoinduced dichroism grating is monitored by diffraction of a cw, horizontally propagating, vertically polarized, 632.8 nm probe beam from a helium-neon laser. The angle (ϕ) of incidence of the probe beam and exit of the diffracted beam with respect to the grating normal satisfies the Bragg condition,

$$\sin\phi = \frac{632.8}{690.0}\sin(\theta/2) \tag{8}$$

so that $\phi = 18.3°$, and the polarization of the diffracted probe light is rotated to *horizontal* (von Jena and Lessing, 1979).

A theoretical expression for the diffraction efficiency (η) of a polarization grating was obtained by extending the theory developed by von Jena and Lessing (1979), and is presented elsewhere (Naimushin et al., 1999b). When the total diffraction efficiency is small ($\eta < 0.01$), as is the case here (and in many other experiments), the result can be very accurately approximated by

$$\eta = \exp\left[-\frac{(2.3)\bar{A}_{\text{probe}}}{\cos\phi}\right]\left(\frac{\pi T}{\lambda_r \cos\phi}\right)^2 \cdot \left[\left(\frac{\Delta[\delta k(t)]}{2}\right)^2 + \left(\frac{\Delta[\delta n(t)]}{2}\right)^2\right] \tag{9}$$

where $\bar{A}_{\text{probe}}$ is an "average" optical density adjusted so that the exponential factor describes the absorptive loss of the probe, T is the sample (or grating) thickness, and λ_r is the probe wavelength in the sample. The quantities $\delta k(t) = k_{+\pi/4}(t) - k_{-\pi/4}(t)$ and $\delta n(t) = n_{+\pi/4}(t) - n_{-\pi/4}(t)$ denote the *local* imaginary and real parts, respectively, of the complex *birefringence* at a particular point in the sample. k_Ω and n_Ω denote imaginary and real parts of the complex *refractive index* for probe light with polarization direction Ω in the plane of the grating. Hence, $\delta k(t)$ is proportional to the photoinduced *dichroism* at a given point in the sample. That is, $\delta k(t) \propto \Delta A_{\parallel}(t) - \Delta A_{\perp}(t)$. The quantity $\Delta[\delta k(t)]$ is the peak-to-null variation in $\delta k(t)$, which varies periodically along the grating, wherein the principal axis of the dichroism is alternately rotated by $+\pi/4$ and $-\pi/4$ with respect to vertical. A similar definition applies to $\Delta[\delta n(t)]$. As noted above, there is no ordinary *thermal* phase grating contribution to $\Delta[\delta n(t)]$. Any contribution of the 1% polarized photobleach (triplet formation) to $\Delta[\delta n(t)]$ is assumed to be negligibly small, so our polarization grating is then purely absorptive. The diffraction efficiency of such an absorptive *polarization* grating is 36 times smaller than that of the corresponding purely absorptive *intensity* grating, in which both write beams have vertical polarization (Naimushin et al., 1999b). However, because an absorptive intensity grating inevitably also exhibits a thermal phase grating, its diffraction efficiency may exceed that of the corresponding polarization grating by considerably more than 36-fold. For one of our samples, the measured ratio was 60-fold. The weak signal of the polarization grating makes alignment and optimization of the experiment both difficult and time-consuming, and requires a great many (~100,000) shots for data acquisition. After considerable effort, the observed initial diffraction efficiency was brought within a factor of 2.6 of the theoretical value calculated from Eq. 9. The $\Delta[\delta k(0)]$ value used in that calculation was evaluated from the measured change in absorbance of the probe beam following a write pulse, when one of the two intersecting write beams was blocked, as described elsewhere (Naimushin et al., 1999b). A significant fraction of this 2.6-fold discrepancy is due to rapid unresolved dye wobble. The remainder is attributed to partial multi-mode character of the pump laser and suboptimal alignment of the beams either at their intersection in the sample or on the most active region of the photomultiplier tube. Such instrumental defects diminish the signal amplitude in a proportional manner, but do *not* alter the time course of the relative decay of the signal. Because Eq. 9 does not *in practice* yield the actual diffraction efficiency (or equivalently the amplitude of the diffracted signal), it is *not* possible to determine the absolute value of the peak-to-null variation in dichroism, $\Delta[\delta k(t)]$, in the sample. This inability to provide the *absolute value* of the dichroism in the sample is the principal disadvantage of the TPG method. This requires an additional disposable parameter in the data analysis. In the case of DNA/MeBl complexes, the initial anisotropy in TPD experiments was often found to be anomalously low (Hogan et al., 1982, 1983; Allison et al., 1989), so rather large adjustments of the ARF parameter in Eq. 3 were required in any case. Hence, the relative disadvantage of TPG experiments with respect to direct TPD experiments is perhaps not so great in this case.

By writing the grating with 690-nm pulses and probing with a 632.8-nm beam, and using appropriate narrow bandpass filters in the detection optics, we have effectively screened out the vast majority of scattered 690-nm light and also the MeBl fluorescence, which is very short-lived ($\lesssim$630 ps) (Naimushin et al., 1999b; Naimushin, 1999). A polarizer in the detection optics passes the horizontally polarized diffracted beam and blocks any vertically polarized probe light, whether scattered or diffracted from an adventitious thermal phase grating, such as might arise from the very small induced CD of the intercalated MeBl (Nordén and Tjernfeld, 1982).

The diffracted probe light is detected by single-photon counting via a photomultiplier and constant fraction discriminator (CFD). The output of the CFD is a nuclear instrumentation module (NIM) standard negative logic pulse of adjustable width, which is set to match the channel width (10 ns) of a transient digitizer-recorder, whose track and hold circuit samples once every 10 ns channel. In this way, every photon detected by the photomultiplier is captured (provided that the maximum count rate does not exceed 0.01 photons/10 ns), and stored in the appropriate recorder channel. Because the dichroism in the sample is monitored by a single detector, both systematic and random errors are significantly reduced compared to direct TPD experiments, in which the dichroism is measured by using two detectors. In particular, systematic errors due to any mismatch in the calibration of the two detectors are completely eliminated, which is crucial for obtaining precise data from the very tail of the decay curve.

The (slow) kinetics of photobleach recovery are measured by blocking one of the excitation pulses (so no grating is created) and monitoring the intensity of transmitted probe light, which is polarized at 54.7° from vertical for these measurements. This is done using a photodiode and the same transient recorder. The diffraction and absorbance signals are transferred to a computer and accumulated between successive shots. Typically, the responses to 50,000 to 100,000 shots are accumulated to provide adequate diffracted signals, but only 1000 accumulated shots are needed to produce excellent triplet decay curves (Naimushin et al., 1999b; Naimushin, 1999).

Least-squares fitting of the transient absorption curves to a double-exponential function typically yields a normalized triplet decay function ($f_T(t)$) consisting of a major component with a lifetime ~10–20 μs, and a minor component with a much longer lifetime, ~70 μs (Naimushin et al., 1999b; Naimushin, 1999). Because the kinetics of photobleach recovery are rather slow compared to the decay of the diffracted signal, and the precision of the $f_T(t)$ data is so great, the determination of $f_T(t)$ contributes negligibly to the error in our final results.

Rotations of the transition dipoles of the unbleached MeBl molecules toward the bleached orientations diminish the local dichroism and cause a decay of the diffracted signal. Likewise, decay of the triplet T_1 states of the bleached molecules back to their ground S_0 states also diminishes the dichroism and diffracted signal. The signal $S(t)$ is the number of accumulated photon counts in each channel and is proportional to the intensity of diffracted probe light, or equivalently to the diffraction efficiency in Eq. 8. Hence, $S(t)$ is proportional to the square of the instantaneous dichroism in the sample, and can be written as (Schurr, 1984; Naimushin et al., 1999b)

$$S(t) = W[r_N(t) f_T(t)]^2, \tag{10}$$

where W is an unknown proportionality constant, $r_N(t) = r(t)/(\text{ARF})(2/5)$ is the *normalized* anisotropy from Eq. 3, and $f_T(t)$ is the *normalized* triplet decay function. All constants that affect the amplitude, but not the shape, of the decay are lumped into the adjustable parameter W. Translational

diffusion generally also contributes to the decay of $S(t)$, but in the present experiments on 200-bp DNA/MeBl complexes, relaxation of the grating by translational diffusion is several hundred times slower than by end-over-end tumbling, so it can be omitted from the data analysis with negligible error. A heterodyne term between a small amount of depolarized scattered light and the diffracted beam ($I_{scat}/I_{diff} < 0.0006$) was expected to contribute ~5% of the initial signal, but was shown to vanish, presumably due to shot-to-shot variations in phase of the grating and its diffracted beam relative to that of the scattered light.

DATA ANALYSIS

Triplet decay function

The measured decay curve is fitted by a double exponential using an iterative nonlinear least-squares method. The fits, shown elsewhere (Naimushin et al., 1999b; Naimushin, 1999), are excellent. The dominant component typically has a lifetime in the range 10–20 μs, and arises from the MeBl triplet state. We have not yet identified the origin of the minor slow component with a very long lifetime, ~70 μs. It could conceivably represent the reoxidation of a small amount of reduced (so called leuko-) MeBl, generated by the write pulses and subsequent photochemistry, back to ground state MeBl. In any case, the kinetics of that process are so slow that it has no significant effect on our results. The best-fit $f_T(t)$ curve in each case is used in the subsequent fitting of Eqs. 10 and 11.

End-over-end tumbling times

As noted above, τ_R can be determined from the TPG data in a manner that is independent of the model or its input parameters, except for the assumed exponential decay of the terminal relaxation process. In that case, we simply fit

$$S(t) = A[\exp[-t/\tau_R]f_T(t)]^2 \qquad (11)$$

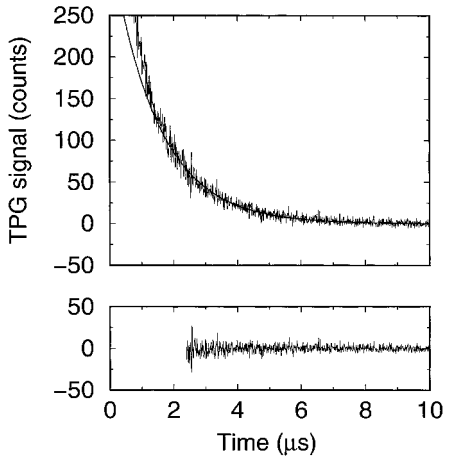

FIGURE 2 $S(t)$ vs. t for a 200-bp DNA in 4 mM ionic strength (*top*). The smooth line is the fit of Eq. 11 to the data at long times. The bottom panel is a plot of the residuals from that fit.

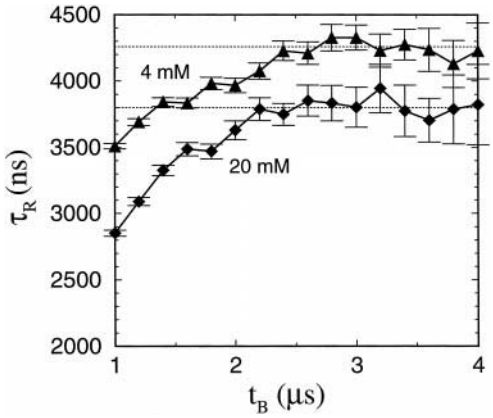

FIGURE 3 τ_R vs. t_B for the 200-bp DNA in two different ionic strengths.

to the experimental data by an iterative nonlinear least-squares procedure. The adjustable parameters are τ_R and the amplitude A. Equation 11 is fitted to the TPG data from different beginning times t_B in the tail of the decay curve out to a final time of 10 μs. A typical fit is shown in Fig. 2, and a plot of the best-fit τ_R vs. t_B is presented in Fig. 3. As expected, the best-fit τ_R rises gradually to a plateau value, and the errors increase as t_B moves progressively farther toward the tail of the decay. The best-fit values of τ_R are taken to be averages of the results along the plateau from $t_B = 2.4$ to 3.4 μs. The best-fit τ_R values of all our samples at different ionic strength and DNA concentration were determined and reported in a separate paper (Naimushin et al., 1999a). Those values most pertinent to the present work are collected in Table 1. Both increasing the ionic strength above 20 mM and decreasing the DNA concentration from 1.5 to 0.75 g/l lead to $\tau_R \cong 3.80$ μs, which suggests that such a value applies when intermolecular interactions are sufficiently weak. The effect of intermolecular interactions to *retard* end-over-end *self*-rotational diffusion, which is probed by the TPG experiment, is analyzed in the other paper (Naimushin et al., 1999a). It is expected that τ_R for the present DNA at much greater dilution in 4 mM ionic strength would be 3.80 μs *or less*.

Evaluation of P_{tot}

We can estimate the total persistence length of our DNA by following the protocol of Hagerman and Zimm (1981).

TABLE 1 Best-fit τ_R values of 200 bp DNA at pH 7.5 at 21°C

[DNA] (g/l)	Ionic Strength (mM)	τ_R (μs)
1.5	4	4.26 ± 0.04
1.5	8	4.00 ± 0.07
1.5	20	3.8 ± 0.05
1.5	47	3.78 ± 0.03
0.75	4	3.80 ± 0.10

They analyzed the ratio $R = \tau_{R(wc)}/\tau_{R(rod)}$, where $\tau_{R(wc)}$ is the average value, either measured or simulated, for a semiflexible filament, and $\tau_{R(rod)}$ is the value calculated for a completely rigid rod of the same contour length by using the Broersma relation (their Eq. 23) with an effective hydrodynamic radius, $R_H = 13$ Å. By using their recommended value, $h = 3.4$ Å, for the rise per bp, we calculate $\tau_{R(rod)} = 5.53$ μs at 294 K in water. When combined with the experimental value, $\tau_R = 3.80$ μs, observed for our least strongly interacting DNAs, the ratio $R = (3.80/5.53) = 0.687$ is obtained. Hagerman and Zimm simulated configurations and computed the $\tau_{R(wc)}$ values for a large number of wormlike chain filaments with appropriately chosen hydrodynamic parameters over a fairly wide range of the ratio, $X \equiv L/P_{tot}$, of contour length to total persistence length. Their numerical results are summarized in a few simple equations (their Eqs. 20–22) that enable one to readily calculate R from X. If we assume that $P_{tot} = 500$ Å, then $X = 680/500 = 1.36$, and the predicted ratio is $R = 0.681$, which is practically identical to the experimental ratio given above. Hagerman (1981, 1988) did not examine such short DNAs in 4 mM ionic strength, but for longer restriction fragments he obtained $P_{tot} = 500$ Å in 4 mM and higher ionic strength. Thus, the best available estimate of P_{tot} of our DNA in 4 mM (and probably also higher) ionic strength is ~500 Å. If intermolecular interactions significantly retard *self*-rotational diffusion in our sample, then the actual P_{tot} of our DNA will be somewhat *smaller*. The essential point is that P_{tot} for our DNA in 4 mM and higher ionic strength does not significantly exceed 500 Å if the analysis of Hagerman and Zimm is quantitatively accurate.

Our most precise and interpretable experimental data pertain to the 1.5 g/l sample in 4 mM ionic strength. The average value $D_R = 1/(6\ \tau_R) = 3.91 \times 10^4\ s^{-1}$ measured for this sample is used in the subsequent analysis of both the FPA and TPD data. The intermolecular hydrodynamic interactions in this twofold more concentrated solution increase τ_R by ~12%, but are assumed not to significantly affect the dynamics of bending. If significant, their effect would be to slow the bending modes and slightly decrease the apparent P_d below the actual value.

Analysis of the FPA data

The horizontally and vertically polarized fluorescence intensities are combined to form the sum ($s(t) = i_V(t) + 2i_H(t)$) and difference ($d(t) = i_V(t) - i_H(t)$) decay curves. These are fitted by convolutions of the measured instrument response function ($e(t)$) with appropriate theoretical model functions:

$$s(t) = \int_0^t dt' e(t - t')S(t') \tag{12}$$

$$d(t) = \int_0^t dt' e(t - t')S(t')r(t') \tag{13}$$

The theoretical sum function is taken to be:

$$S(t) = A_s\delta(t) + S_1 e^{-t/\tau_1} + S_2 e^{-t/\tau_2} \tag{14}$$

wherein the delta function accounts for Raman scattering. The best-fit relaxation times, $\tau_1 \cong 21.8$ ns and $\tau_2 \cong 1.5$–2.0 ns, correspond to intercalated and nonintercalated ethidium, respectively. The contributions of Raman scattering and nonintercalated ethidium are suppressed by omitting the first 4 ns from the fit of the difference data. The anisotropy function $r(t)$ is given by Eqs. 3–7. The fit was performed for a wide range of *assumed* P_d values from 500 to 5000 Å. Adjustable parameters in the fit were the torsion elastic constant α and ARF. The fixed input parameters, in addition to D_R for end-over-end tumbling, were listed above. The fits were performed over four different time spans, 0–16, 0–32, 0–70, and 0–120 ns. For each choice of P_d, the optimum α-value "varied" with time span in much the same way as reported previously for the linear 181-bp DNA (Heath et al., 1996a). The 0–16-ns fit and to a lesser extent the 0–32-ns fit gave somewhat higher α values than the 0–70- and 0–120-ns fits. The results from the latter two time spans were averaged to obtain the best-fit value of α for each assumed value of P_d. Essentially the same reduced χ^2 values in the range 1.00–1.05 were obtained for all assumed values of P_d from 500 to 5000 Å (or more). The best-fit α values are plotted versus $1/P_d$ in Fig. 4. This empirical relation is the main result of our FPA measurements on the DNA ethidium complexes, and serves to eliminate α as an independent variable in the subsequent analysis of the TPG data.

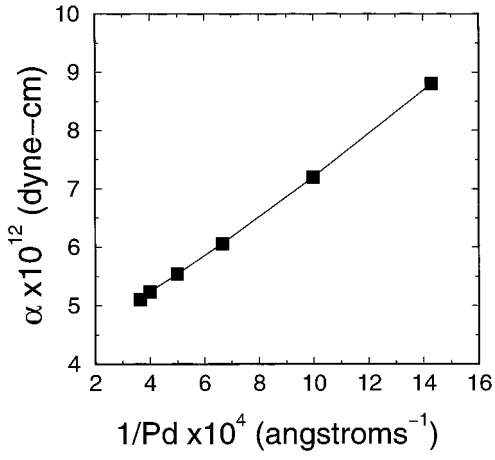

FIGURE 4 Best-fit α vs. $1/P_d$ from fit of Eqs. 3–7 to the FPA data for the 200-bp DNA in 4 mM ionic strength. For each assumed value of P_d a best-fit value of α was obtained from the fit.

Redetermination of ε

Hogan et al. obtained the value $\varepsilon = 72°$ by measuring the limiting value of the reduced linear dichroism, LD^r (Hogan et al., 1982). Their limiting LD^r value was analyzed without taking dye wobble into account. From the reported value $\varepsilon = 72°$, the unreported experimental datum, $LD^r = -1.05$, can be recovered by using the following relation with ARF = 1.0,

$$LD^r = -1.05 = 3(\mathrm{ARF}\, I_0(\infty))^{1/2} \tag{15}$$

A protocol for estimating both ε and the root-mean-squared amplitude of isotropic wobble, $\sigma = \langle \delta\varepsilon^2 \rangle^{1/2}$, from LD^r and the ARF value derived from FPA measurements was described previously (Schurr and Fujimoto, 1988). The value ARF = 0.75 for DNA/MeBl complexes in 4 mM ionic strength is obtained by extrapolating the ARF versus ionic strength data of Fujimoto et al. (1994a). The analysis proceeds by determining numerically the pairs of values (ε, $\langle \delta\varepsilon^2 \rangle$) that simultaneously satisfy Eq. 15, and also the relation, ARF = 0.75. The results are shown in Fig. 5, from which the solution $\varepsilon = 75°$ is readily apparent. This value will be used in the subsequent analysis of TPG data. If the smaller value, $\varepsilon = 72°$, were used, the best-fit value of P_d would be somewhat larger than that obtained below.

Analysis of the entire TPG decay

The timing of the transient digitizer is such that the write pulses occur primarily within a single 10-ns channel with only ~15% overlap into the channels on either side. Consequently, it is not actually necessary to deconvolute the TPG data, provided the data in the first two channels *after* the peak of the signal are ignored. The TPG data from 30 ns to 10 μs after the peak of the excitation pulse are fitted by Eq. 10, using the best-fit $f_T(t)$ and the normalized $r_N(t)$ reckoned from Eqs. 3–7. The 0-ns channel was taken to be that with maximum signal, which occurs 10 ns after the peak of the excitation pulse. Thus, the fits begin with the 20-ns channel, which occurs 30 ns after the peak of the excitation pulse, and the theoretical value is appropriate for the 30-ns delay of that channel. This delay of the start of the fit until 30 ns, where the slope of $r_N(t)$ is considerably reduced, serves to diminish the error arising from the variable location of the write pulses within the 10-ns channel in which they occur. Although not necessary, a convolution of the theoretical curve with a three-point excitation function was used in the final fits. Before fitting, a very small first-order correction is applied to the data in each channel to account for missing counts that arrived during the 10-ns dead time following each photon. Three experimental decay curves for the same conditions were normalized to the same total number of counts and fitted simultaneously with the same theoretical curve. After determining τ_R, the remaining adjustable parameters are P_d, W, and the excess azimuthal wobble, $\langle \delta\zeta^2 \rangle$ in Eqs. 5a–c, which is initially taken to be zero. The fit is conducted by a grid search, beginning with selected values of P_d and their corresponding α values, as determined from the empirical relation in Fig. 4. Theoretical values of $(r_N(t) f_T(t))^2$ and $S(t)^{th}$ are then calculated for each channel, and the reduced chi-squared

$$\chi_r^2 = (1/(M-n)) \sum_{j=1}^{M} (S(t_j)^{exp} - S(t_j)^{th})^2 \tag{16}$$

is calculated for all M data points, where n is the number of disposable parameters. A contour plot of χ_r^2 vs. P_d and W is obtained for the isotropic wobble model with $\varepsilon = 75°$ and $\langle \delta\zeta^2 \rangle = 0$. In this case such a plot is not particularly informative, since instead of a more or less circular basin it is a descending canyon that drains toward higher P_d nearly parallel to the P_d-axis. A more useful representation, especially when three variables are adjustable, is to plot the minimum value of χ_r^2 for each choice of P_d vs. P_d. This projects the optimum χ_r^2 values along the bottom of the canyon or basin onto the $\chi_r^2 - P_d$ plane. For the isotropic wobble model with $\varepsilon = 75°$, the optimum χ^2 vs. P_d curve descends monotonically with decreasing slope all the way from one grid boundary (P_d = 500 Å) to the other (P_d = 5000 Å) (not shown). Throughout this region χ_r^2 remains so high (≳2.39344) that the fits are rather poor (not shown). For example, $\chi_r^2 = 4.42298$ for the optimum fit at P_d = 2000 Å. The poor quality of the fit is confirmed by visually comparing the optimum theoretical curves for different choices of P_d with the experimental curves (not shown). The essential problem is that the theoretical curve descends too rapidly from 30 ns to ~800 ns, which implies that the relative amplitudes of the $n = 1$ and 2 terms in Eq. 3 are too large compared to that of the $n = 0$ term.

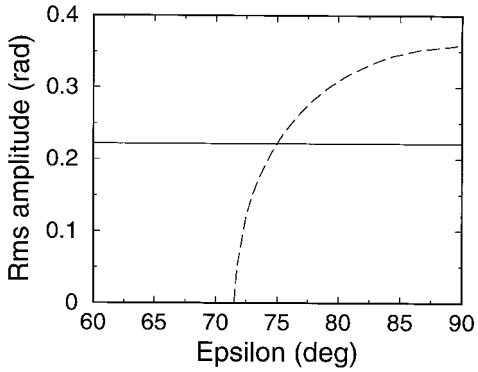

FIGURE 5 Root-mean-squared amplitude of isotropic wobble ($\langle \delta\varepsilon^2 \rangle^{1/2}$) vs. ε. The solid line is a plot of (ε, $\langle \delta\varepsilon^2 \rangle^{1/2}$) pairs that satisfy ARF = 0.75. The dashed line is a plot of (ε, $\langle \delta\varepsilon^2 \rangle^{1/2}$) pairs that satisfy $LD^r = -1.05$. At the intersection, $\varepsilon = 75°$.

Variation of P_d, W, and ε

The possibility remains that the value $\varepsilon = 75°$ is not appropriate for the TPG (or TPD) experiment. All bound MeBl molecules participate nearly equally in the *absorbance* detected LD^r, but only one particular kind of binding site dominates the photobleaching and TPG (or TPD) signal, and that is a minority species. That species conceivably has a polar angle ε that differs significantly from the average value reckoned from the LD^r. Hence, we varied P_d, W, and ε in the fitting protocol again via a grid search. The curve of optimum χ_r^2 vs. P_d again exhibits no minimum between the grid boundaries, but instead declines with decreasing slope from $P_d = 500$ Å to $P_d = 5000$ Å (not shown). Throughout this region, the best-fit ε exceeds 76.4°. The optimum χ_r^2 values are now much lower and the fits greatly improved, but they are still not altogether satisfactory. A comparison of the optimum fit for $P_d = 2000$ Å ($\varepsilon = 79.7°$, $W = 7084$) with the experimental data is shown in Fig. 6. The theoretical curve still descends too rapidly from 30 to 800 ns. For this curve, $\chi_r^2 = 2.38418$. χ_r^2 rises rapidly with decreasing P_d, so the discrimination against significantly lower values, $P_d \leq 1500$ Å, appears to be very great.

Unsuccessful attempts to improve the fit

Several modifications of the model were undertaken in unsuccessful attempts to *significantly* improve the fit.

1. The dye was assumed to undergo 7° of isotropic wobble, like ethidium, plus the necessary amplitude of excess azimuthal wobble to attain the extrapolated ARF = 0.75 *for the* FPA of DNA/MeBl complexes in 4 mM ionic strength (Fujimoto et al., 1994a). Although this improved the fit slightly, it didn't go nearly far enough;
2. A distribution of the polar angle ε over a span of up to $\pm 10°$ was admitted, but that had almost no effect on either the quality of the fit or the optimum parameters. Hence this protocol was eschewed;
3. Two different binding sites (A and B) with very different polar angles were admitted. The polar angle ε_A of species A was allowed to vary from 65 to 90°, whereas ε_B of species B was allowed to vary from 0 to 45°. Species A would correspond to the normally intercalated MeBl and B to an outside bound MeBl. The relative fraction of species B was allowed to vary from 0 to 1.0. The fit improved significantly only when both species comprised roughly equal fractions of the dye. However, so large a fraction of outside bound dye is incompatible with certain results of Fujimoto et al. (1994a). Specifically, in 10 mM Tris, 0.01 mM Na_2 EDTA, pH 7.5, at 20°C both negatively supercoiled and linear DNA/MeBl complexes exhibit very similar relative amplitudes and decay times of all three observed fluorescence components. However, the binding affinity of DNA for intercalated MeBl *relative* to outside bound MeBl is much greater in negatively supercoiled than in linear DNAs. Hence, the invariance of the relative populations to supercoiling implies that all three fluorescence components must arise from the same kind of site, either intercalated or outside bound. Unwinding studies at low ionic strength show that a majority of the MeBl is in fact intercalated, so all three fluorescent sites must be intercalated with similar unwinding angles. The slight differences in relative fluorescence amplitudes between the linear and supercoiled DNAs allow for at most only a few percent of outside bound MeBl. Such a small fraction of outside bound dye does not significantly improve the fit, so this model was eschewed;
4. A distribution of τ_R times was admitted. This was not done in earlier studies, because the bending motions were believed to explore and average all relevant configurations in a time much less than τ_R. Because $\tau_R \simeq 4.3$ μs exceeds by ~14-fold the longest dynamic bending relaxation time, $T_2 \simeq 325$ ns, for the present DNA, this is a good approximation *in regard to dynamic bending*. However, the present DNA also exhibits sequence-dependent permanent bends and effectively frozen slowly relaxing bends. The former bends contribute to reduce τ_R by the same factor for every molecule. However, the frozen slowly relaxing bends will vary from one molecule to another, and thereby generate a distribution of τ_R. A protocol for calculating a suitable distribution of τ_R is described in Appendix B. Incorporation of this distribution produced only a very slight improvement in the fit and very little effect on the best-fit parameters. Never-

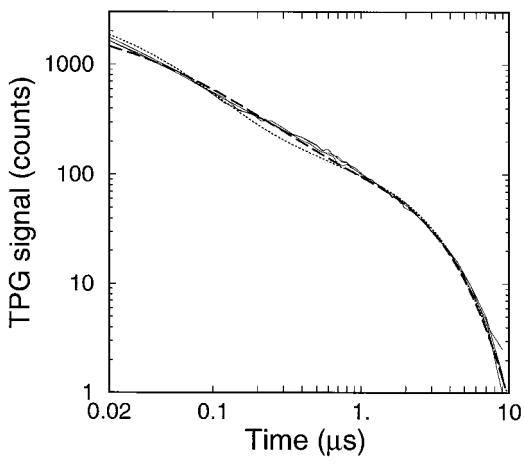

FIGURE 6 TPG signal $S(t)$ versus time. The three thin solid lines are smoothed data for three different measurements on a 200-bp DNA in 4 mM ionic strength. The dotted line is the best fit of Eq. 10 to the data, when it is assumed that $P_d = 2000$ Å, but ε and W are adjustable, and the MeBl wobble is isotropic. When $P_d = 2000$ Å, the optimum values are $\varepsilon = 79.7°$, $W = 7084$, $\chi_r^2 = 2.38418$. The dashed line is the global best fit of Eq. 10 to the data when it is assumed that $\varepsilon = 75°$, but P_d, $\langle \delta\zeta^2 \rangle^{1/2}$, and W are all adjustable. The globally optimum parameters are $P_d = 2000$ Å, $\langle \delta\zeta^2 \rangle^{1/2} = 25°$, $W = 11{,}100$, $\chi_r^2 = 1.94862$.

theless, this procedure was retained in the subsequent fitting protocol for the sake of self-consistency.

Admission of arbitrarily large excess azimuthal wobble

Finally, we admit arbitrarily large azimuthal wobble. This possibility was considered for three reasons. 1) Excess azimuthal wobble *will* decrease the relative amplitudes of the $n = 1$ and 2 terms in Eq. 3, and thereby improve the fit. 2) Anomalously low ARF values in TPD experiments on DNA/MeBl complexes were often observed, especially for GC-rich DNAs (Allison et al., 1989; Hogan et al., 1982, 1983). The implied large amplitudes of rapid local angular motion of the transition dipole more likely reflect azimuthal wobble (around the local symmetry axis) than polar wobble. 3) In the case of the FPA of DNA/MeBl complexes, the ARF value decreases significantly with increasing temperature (Fujimoto et al., 1994a), in contrast to DNA/ethidium complexes, where ARF is practically independent of temperature. This suggests that the amplitude of (presumably azimuthal) dye wobble in DNA/MeBl complexes is for some reason surprisingly sensitive to thermal energy. An important difference between FPA and TPG (or TPD) experiments on DNA/MeBl complexes is that in the FPA only a single photon is absorbed from the excitation pulse by the emitting MeBl, whereas in the TPG (and TPD) experiments, typically several photons have been absorbed from the excitation pulse prior to the photon that leads to photobleaching. As most of the energy from previously absorbed photons is internally converted, the photobleaching then typically occurs in a locally preheated molecule. We suspect that the intercalation site is temporarily enlarged in some way by this local preheating to allow a substantially larger amplitude of azimuthal wobble. If the lifetime of the enlarged intercalation site is >10 μs, then Eqs. 5a–c apply as is. However, if the enlarged intercalation site narrows back down to the normal site typical of the FPA excited state (with ARF = 0.75 and $\langle\delta\zeta^2\rangle = 0$) within 30 ns, as seems likely, then the $\langle\delta\zeta^2\rangle$ in Eqs. 5b and c must be replaced by $\langle\delta\zeta^2\rangle/2$, as described in Results and Discussion. In practice we simply use equations 5a–c directly in the fitting routine, and interpret the best-fit $\langle\delta\zeta^2\rangle$ in the appropriate way for either scenario at the end. The fitting is again conducted by a grid search along the coordinates of the three adjustable parameters, P_d, $\langle\delta\zeta^2\rangle$, and W with ε fixed at 75°. With this model, a true minimum occurs in the curve of the optimum χ_r^2 vs. P_d, as shown in Fig. 7. The minimum value, $\chi_r^2 = 1.94862$, is found for $P_d = 2000$ Å, $\alpha = 5.54 \times 10^{-12}$ dyne cm, $\langle\delta\zeta^2\rangle^{1/2} = 25°$, and $W = 11{,}000$. These optimum values are collected in Table 2. With this value of $\langle\delta\zeta^2\rangle^{1/2}$, the ratio, $ARF_{tot}/ARF_{iso} = 0.61$, where ARF_{tot} is the total ARF and ARF_{iso} is the factor due to isotropic wobble, which is lumped in with W. A comparison of the optimum theoretical curve for this azimuthal-wobble model with the experimental signals is shown in Fig. 6. The azimuthal-wobble model clearly provides a much more satisfactory fit than the isotropic wobble model with $P_d = 2000$ Å and $\varepsilon = 79.7°$. This is also evidenced by the substantial reduction in reduced χ_r^2 from 2.38418 to 1.94862. This difference is statistically overwhelming when account is taken of the very large number of data points ($N = 2994$) in the three experimental curves.

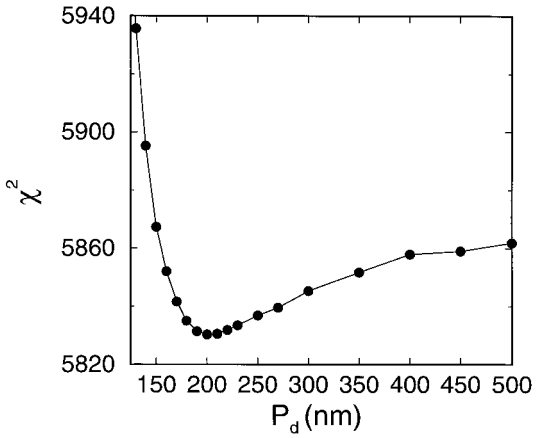

FIGURE 7 Total χ^2 vs. P_d for the fit of Eq. 10 to the data in Fig. 6 under the assumption that $\varepsilon = 75°$, but P_d, $\langle\delta\zeta^2\rangle^{1/2}$, and W are all adjustable.

In the final fits of this azimuthal wobble model, the theoretical curve was convoluted with a three-channel excitation function. The effects of such a convolution on the results were exceedingly minor, and this was done primarily for the sake of completeness.

RESULTS AND DISCUSSION

P_{tot} and P_d

For the first time, practically independent *and* more or less unambiguous measurements pertaining to P_{tot} and P_d are available for the same DNA molecule. These values apply for this particular 200-bp DNA in 4 mM ionic strength at 21°C. The $\tau_R \simeq 3.80$ μs of the 0.75 g/l DNA sample yields $P_{tot} \simeq 500$ Å. The fit of the isotropic-wobble model with variable ε to the TPG (and FPA) data yields only a lower bound $P_d \geq 1500$ Å. However, the fit of the azimuthal-wobble model to the same data yields $P_d = 2000(-200, +300)$ Å, where the statistical errors are conservatively set at about twice the square root of the variance, which is estimated from the variation of χ^2 with P_d along the optimum χ^2 vs. P_d curve.

TABLE 2 Best-fit parameters for the azimuthal wobble model

N (bp)	L (Å)	P_{tot} (Å)	P_d (Å)	$\alpha \times 10^{12}$ (dyne cm)	$\langle\delta\zeta^2\rangle^{1/2}$ (deg)
200	680	500	2000	5.54	25

The ratio of the probabilities that any two optimum solutions for P_d, $\langle\delta\zeta^2\rangle$, and W with different values of P_d give rise to the data is given approximately by

$$P(P_{d2})/P(P_{d1}) = \exp[(\chi_2^2 - \chi_1^2)/2] \qquad (18)$$

wherein $\chi_j^2 = \eta\,\chi_{rj}^2$ is the *total* chi-squared for the solution $j(j = 1, 2)$, χ_{rj}^2 is its *reduced* chi-squared, and $\eta = M - n$ is the number of data points ($M = 2994$) minus the number of disposable parameters ($n = 2$). For example, using $\chi_{r1}^2 = 1.94862$ for $P_d = 2000$ Å and $\chi_{r2}^2 = 1.95589$ for $P_d = 1600$ Å, we obtain $P(1600)/P(2000) = 1.9 \times 10^{-5}$. By this criterion, $P_d = 1600$ Å is ~50,000 times less likely to have given rise to the data than is $P_d = 2000$ Å. The optimal χ_r^2 increases and the probability ratio $P(P_{d2})/P(2000)$ declines rapidly and monotonically as P_{d2} descends further. In a purely statistical sense, these data effectively preclude any value of P_d outside the range 1600–2700 Å under the prevailing conditions.

The present optimum value, $P_d = 2000$ Å, in 4 mM ionic strength at 21°C is only slightly smaller than the value $P_d \cong 2100$ Å, in 2 mM ionic strength at 21°C, which was obtained by *assuming* that the rapid initial transient in the TED off-field decay represents the longest bending normal mode (Song and Schurr, 1990). Because the present data so strongly preclude P_d values as low as 500 Å, and select a value close to 2100 Å, that assumption now becomes the most likely interpretation of the TED data. This in turn suggests that the electric field in the TED experiments acts in a nonlinear manner to enhance the longest bending normal mode, presumably in the manner suggested by Elvingson (1992), because that is apparently the only way in which it can appear with sufficient amplitude in the TED off-field decay (Heath et al., 1995).

Torsional rigidity

The optimum torsion elastic constant, $\alpha = 5.54 \times 10^{-12}$ dyne cm, corresponds to a torsional rigidity, $C = h\alpha = 1.9 \times 10^{-19}$ dyne cm^2, where $h = 3.4$ Å is the rise per bp. This lies within the range of values obtained by Taylor and Hagerman (1990) from cyclization kinetics of 350–360 bp DNAs, and is within experimental error of the value $C = 2.0 \times 10^{-19}$ dyne cm^2, which was shown to quantitatively predict the supercoiling free energies, structure factors, and translational diffusion coefficients of a supercoiled DNA (Gebe et al., 1995, 1996; Delrow et al., 1997). The FPA data on the present DNA/ethidium complexes indicate that the torsional rigidity of the present sample is ~5% lower than that of the 181-bp DNA studied by Heath et al. (1996a) in 100 mM ionic strength, assuming that both samples have the same P_d.

RMS Wobble

In the TPG experiment the value $\langle\delta\zeta^2\rangle^{1/2} = 25°$ pertains to excess (beyond isotropic) azimuthal wobble of the intercalated MeBl in its S_0 ground state. This value is too large to be compatible with the measured ARF = 0.75 for intercalated MeBl in its S_1 excited state in the FPA experiments (Fujimoto et al., 1994a). Either the RMS amplitude of azimuthal dye wobble is normally much larger for the S_0 state than for S_1, which seems unlikely, or else it is peculiarly enhanced in the TPG and TPD experiments. As noted above, in a TPG or TPD experiment, the MeBl typically absorbs several photons during the same 5-ns excitation pulse that internally convert before absorbing the photon that leads to triplet formation and photobleaching. Consequently, the complex has been preheated. A rise in local temperature due to such preheating that is accompanied by some minor structural change provides a plausible explanation of the present results.

The expressions 5a–c are obtained under the assumption that $\delta\zeta(t)$ is a stationary Gaussian random variable, for which $\langle\delta\zeta(0)^2\rangle = \langle\delta\zeta(t)^2\rangle = \langle\delta\zeta^2\rangle$. In fact, the $\exp[-n^2\langle\delta\zeta^2\rangle]$ factors follow from

$$\langle\exp[in(\delta\zeta(0) - \delta\zeta(t))]\rangle = \exp[-n^2(\langle\delta\zeta(0)^2\rangle + \langle\delta\zeta(t)^2\rangle)/2]$$
$$= \exp[-n^2\langle\delta\zeta^2\rangle],$$

whenever t sufficiently exceeds the dye wobble relaxation time ($\tau_W \simeq 200$ ps) that the correlation function $\langle\delta\zeta(0)\,\delta\zeta(t)\rangle = \langle\delta\zeta^2\rangle\exp[-t/\tau_W]$ effectively vanishes. Use of $\exp[-n^2\langle\delta^2\rangle]$ requires the stationarity condition to hold for all times examined (up to 10 μs). Because the heat deposited in the DNA surely diffuses away on a time scale much less than 10 μs (or even 5 ns) the existence of an enlarged binding site with enhanced azimuthal wobble for so long a time could occur only if there were some persistence of metastable structure at the binding site. The likelihood of such a scenario is difficult to assess.

At the other extreme, the perturbed binding site might relax toward its unheated equilibrium conformation at a rate that is insufficient to equilibrate within the 5-ns excitation pulse, but suffices to equilibrate within the first 30 ns after the pulse. In this case, the variance $\langle\delta\zeta(t)^2\rangle$ of the *excess* azimuthal wobble is expected to decrease from $\langle\delta\zeta(0)^2\rangle$ to 0 in a variance relaxation time τ_V in the range 5 ns $\leq \tau_V \lesssim 30$ ns. Because $\tau_W \ll \tau_V$, it is reasonable to regard $\delta\zeta(t)$ as a nonstationary, but still Gaussian, random variable with a correlation function $\langle\delta\zeta(0)\,\delta\zeta(t)\rangle$ that still vanishes for $t \gg \tau_W$. In such a case, for $t > \tau_V$ one has $\langle\delta\zeta(0)^2\rangle + \langle\delta\zeta(t)^2\rangle = \langle\delta\zeta(0)^2\rangle + 0 = \langle\delta\zeta^2\rangle$, and the $\exp[-n^2\langle\delta\zeta^2\rangle]$ factors in Eqs. 5b and c must be replaced by $\exp[-n^2\langle\delta\zeta^2\rangle/2]$. In this scenario the RMS amplitude of wobble just before absorbing the photobleaching photon is $(\sqrt{2})\cdot 25° = 35°$, but that relaxes to zero during the early stages of the anisotropy decay ($t < \tau_V \simeq 30$ ns). We have not fitted the TPG data to

an intermediate model in which the variance of the enhanced azimuthal wobble relaxes with a time τ_V in the range 5 ns $\lesssim \tau_V \lesssim$ 10 μs, because we are reluctant to introduce another adjustable parameter, but that remains a possibility.

P_{sr} and the slowly relaxing bends

When the present estimates P_{tot} = 500 Å and P_d = 2000 Å are used along with the Schellman-Harvey (SH) prediction, P_{pb} = 1370 Å, in Eq. 1, there results P_{sr} = 1300 Å. The essential point is that P_{sr} is *not* infinite, and that all three kinds of bends make comparable contributions to $1/P_{tot}$. This establishes, albeit indirectly, that 1) slowly relaxing fluctuations in an equilibrium between differently curved conformations *do* contribute significantly to $1/P_{tot}$, and 2) the bending rigidity of DNA is itself a relaxing quantity, such that its equilibrium value at long times, $A_{eq} = k_BT/(1/P_d + 1/P_{sr})$, is only ~40% of its dynamic value at short times, $A_d = k_BT\,P_d$, and corresponds to a flexural persistence length, $P_{eq} = (1/P_d + 1/P_{sr})^{-1}$ = 788 Å. Two observations suggest that 1300 Å likely *overestimates* the actual value of P_{sr}. 1) Modeling the measured *j*-factors for cyclization of small circles typically yields P_{eq} = 500 Å (Shimada and Yamakawa, 1984; Hagerman and Ramadevi, 1990; Taylor and Hagerman, 1990; Hodges-Garcia and Hagerman, 1995; Kahn and Crothers, 1998). Combining P_{eq} = 500 Å with P_d = 2000 Å then yields P_{sr} = 667 Å, which is only about half of the 1300 Å estimate. This (less conservative) value assigns an even greater contribution of slowly relaxing bends to the mean-squared bending of DNA and the reduction of its equilibrium bending modulus below P_d. 2) P_{pb} *for the present DNA molecule* probably exceeds the SH prediction, which is obtained by averaging over a much longer and more varied sequence than that of our 200-bp DNA. In fact, the present 200-bp molecule comes from a region of pBR322 (position 233 to 432) that was shown *not* to exhibit anomalous electrophoretic mobilities in polyacrylamide gels (Stellwagen, 1983), and in electrophoretic comparisons with different standards of known length also in polyacrylamide gels gave no evidence of abnormal mobility or permanent bend. Thus, our DNA is likely to be somewhat straighter than the average sequence for which the SH prediction applies, so P_{pb} for our molecule probably exceeds the SH prediction. Hence, the P_{sr} = 1300 Å estimated from Eq. 1 by using the SH prediction for P_{pb} likely represents an upper bound.

We previously analyzed the effects of imposing a *small* uniform strain on a chain of twisting (or bending) springs, each of which fluctuates between two states with different *intrinsic* twists (or bends) and torque constants, and exhibits average equilibrium twist ϕ_o (or bend θ_o) (Delrow et al., 1997). When the *intrinsic* bends of the two states differ significantly, this model predicts that 1) a *small* uniform bending strain (θ–θ_o per spring) shifts the conformational equilibrium to order θ–θ_o, so that 2) the bending rigidity declines from the dynamic (frozen equilibrium) value A_d to the equilibrium value A_{eq} on the time scale of the equilibration process. This model accounts for both the observed alteration of the average secondary structure by imposed bending strain (Heath et al., 1996a), and the present finding that A_d substantially exceeds A_{eq}. When the two states exhibit practically the same *intrinsic twist*, but different torsion constants, a *small* imposed twisting strain (ϕ–ϕ_o per spring) does *not* alter the conformational equilibrium to order ϕ–ϕ_o (but instead to order $(\phi$–$\phi_o)^2$), so the equilibrium remains nearly frozen and does *not* reduce the equilibrium torsion constant significantly below the dynamic value (Delrow et al., 1997). This model accounts for the (near) equivalence of the dynamic and equilibrium values of the torsion constant, which is evident in Fig. 1, wherein both equilibrium and dynamic methods yield comparable results. These considerations suggest that the two interconverting states exhibit significantly different intrinsic bends, but similar intrinsic twists.

Domain size

From the upper bound, P_{sr} = 1300 Å, we estimate a lower bound for the average domain size, *m*, of the coherently bent conformation in the following way. Each domain of the coherently bent state is assumed to exhibit a fixed planar bend (θ_1 per bp). The total bend per domain is then $m\theta_1$. For simplicity, the duplex filament is divided into sections of *m* bp. Within each section an all-or-none equilibrium between coherently bent (b) and straight (s) conformations prevails, that is, s $\rightleftarrows$ b, with associated equilibrium constant $K = f_b^o/f_s^o$, where $f_b^o = K/K + 1$ and $f_s^o = 1/(K + 1)$ are the equilibrium fractions of the time that each section spends in its b and s states. This equilibrium is illustrated schematically in Fig. 8. To estimate $1/P_{sr}$, the contributions of dynamic bending must be omitted, so every section exhibits either its intrinsically straight or coherently bent conformation. The total contribution of slowly relaxing *fluctuations* in the s $\rightleftarrows$ b equilibrium to P_{sr} is estimated by omitting the contribution of that equilibrium to the *average* curvature, which does not relax and must be counted as part of the permanent bend contribution to P_{pb}. We adopt the approximate expression given in Eq. A6 of Appendix A. When P_{sr} and θ_1 are known, Eq. A6 yields a *minimum* solution for *m*

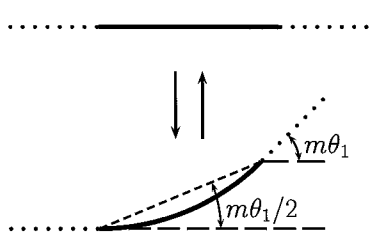

FIGURE 8 Diagram of straight $\Leftrightarrow$ bent equilibrium in domains.

as a function of K, which provides a lower bound estimate of the domain size. The threshold θ_1 required to stabilize the alternative secondary structure, which is induced by the bending strain in small circles (cf. Fig. 1), must lie between 360/360 = 1.0 and 360/247 = 1.46°/bp. The largest estimates of P_{sr} and θ_1 yield the most conservative (smallest) estimate of m. After P_{sr} = 1300 Å and $\theta_1 = (1.46)\pi/180 =$ 0.0254 radian are substituted in Eq. A6, the values of m corresponding to a series of assumed K values are determined numerically via a grid search. Various assumed K values and their corresponding solutions for m are indicated in Table 3. The lower bound value is $[m]_{min}$ = 55 bp, and occurs between K = 0.4 and K = 0.6. There is no solution for $K \lesssim 0.07$, in which case there are evidently too few bent domains to reduce P_{sr} from infinity to 1300 Å.

The present data imply a minimum average domain size of several turns. If $K \lesssim 0.10$, as is not unlikely, then the actual domain size exceeds 100 bp.

Nature of the coherently bent state

Because the coherent bend of the alternative curved state extends over several turns, it is almost certainly superhelical rather than planar. The question arises whether this bend or superhelicity is directional or, equivalently, phase-locked to the azimuthal orientation of the duplex. The meaning of this question is illustrated in Fig. 9. If this curved state is identified with that induced by the bending strain in small DNA circles ($N \leq 250$ bp), then its curvature is *not* directional and *not* phase-locked to the azimuthal orientation of the filament, because the uniform mode of azimuthal spinning is definitely *not* frozen out in the 181-bp circles studied by Heath et al. (1996a). We suspect that this kind of non-phase-locked superhelical curvature is the result of incommensuration and consequent frustration manifested by differential tensions and compressions among the four subfilaments (two base columns and two backbone chains) of DNA. When such internal stresses are relieved by nonlinear (nonharmonic) restoring forces, quasi-periodic variations in the structural parameters of successive basepairs will generally arise and cause a superhelicity that can be translated anywhere along the helix, or equivalently can adopt any phase angle with respect to the azimuthal orientation of the duplex filament, at nearly constant potential energy.

TABLE 3 Domain sizes for different values of K, when P_{sr} = 1300 Å

K	m (bp)
0.07	187
0.08	149
0.10	116
0.20	71
0.30	60
0.40	56
0.50	55
0.60	56
0.70	58
0.80	60
1.00	65
2.00	102
3.00	140
5.00	187
10.00	220

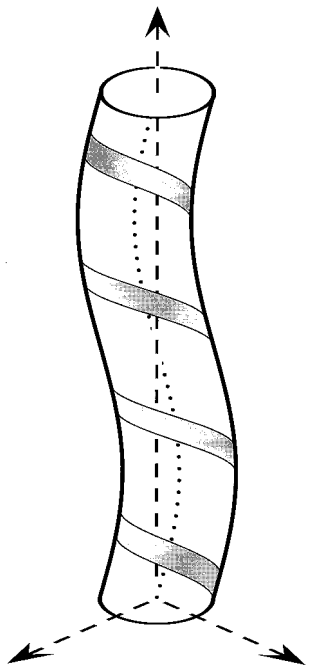

FIGURE 9 Model of intrinsically superhelical linear DNA. The local symmetry axis of the DNA is held fixed at the position of the dotted line, while everywhere the duplex undergoes a uniform azimuthal rotation around that, like the rotation of a speedometer cable in its curved sheath. If the variation of the potential-of-mean-force with phase angle (ϕ) of that azimuthal rotation over the interval 0 to 2π is small compared to k_BT, then such a rotation can occur freely during Brownian motion and the azimuthal orientation of the duplex is not phase-locked to the orientation of the superhelix. In that case, the superhelical curvature is nondirectional. However, if the potential-of-mean-force exhibits one or more barriers greater than k_BT as ϕ varies from 0 to 2π, then such a rotation will be substantially hindered during Brownian motion and the azimuthal orientation of the duplex will be at least partially phase-locked to the orientation of the superhelix. In that case the superhelical curvature is directional.

APPENDIX A

An approximate expression for P_{sr}

With each domain of m bp we associate a bond vector $\mathbf{b}_j$, $j = 1, \ldots \infty$, which has the length $b_s = mh$, if the domain is in the straight (s) conformation, but is somewhat shorter if the domain is in the bent (b) state. When in the b state the entire domain is assumed to bend uniformly in a single plane, which contains any entering or exiting straight section, about either of which the plane can be rotated by the full 2π provided the other moves as the plane rotates. The angle between the tangent vectors at the beginning and end of a bent domain is $m\theta_1$. The bond vector $\mathbf{b}$ of a bent

domain is the chord spanning the arc of the bend, which has length $b_b = (h/\theta_1) \cdot 2|\sin(m\theta_1/2)| \le mh$. This bond vector of the bent state makes angles $m\theta_1/2$ with both the beginning and ending tangent vectors of the arc. We *assume* that relatively minor error is incurred by 1) averaging the bond vector lengths separately from the angular configurations of those same bond vectors, and 2) neglecting the correlations between adjacent pairs of bends that occur in this model. Under these assumptions, this model should behave as if its effective bending potential were isotropic and centrosymmetric, and P_{sr} takes the form

$$P_{sr} = \frac{\langle|\mathbf{b}|\rangle}{1 - \langle\cos[\beta_m - \langle\beta_m\rangle]\rangle} \tag{A1}$$

where

$$\begin{aligned}\langle|\mathbf{b}|\rangle &= f_s^o\, b_s + f_b^o\, b_b \\ &= mh/(K+1) + (K/(K+1))(h/\theta_1)2|\sin(m\theta_1/2)|\end{aligned} \tag{A2}$$

is the average bond vector length, which is computed using $f_s^o = 1/(K+1)$ and $f_b^o = K/(K+1)$. The quantity β_m is the actual angle between $\mathbf{b}_j$ and $\mathbf{b}_{j+1}$, which depends on the states of the j and $j+1$ domains, and $\langle\beta_m\rangle$ is the average of β_m, which contributes to P_{pb}, and must be subtracted to isolate the contribution of fluctuations in the s $\rightleftarrows$ b equilibrium. The averaging is performed over all four joint states of the j and $j+1$ domains: 1) $s_j\ s_{j+1}$; 2) $s_j\ b_{j+1}$; 3) $b_j\ s_{j+1}$; and 4) $b_j\ b_{j+1}$, which occur with the respective probabilities 1) $f_s^{o2} = (1/K+1)^2$; $f_s^o f_b^o = K/(K+1)^2$; 3) $f_b^o f_s^o = K/(K+1)^2$; 4) $f_b^{o2} = (K/(K+1))^2$; and exhibit the respective β_m angles: 1) 0; 2) $m\theta_1/2$; 3) $m\theta_1/2$; 4) $m\theta_1|\cos[\phi/2]|$; where ϕ is the dihedral angle by which the plane of the $j+1$ bend is rotated with respect to that of the j bend. Expression 4) is valid when $m\theta_1$ is not too large. Before proceeding, we *preaverage* over ϕ to obtain

$$\langle|\cos[\phi/2]|\rangle = \frac{1}{\pi}\int_0^{\pi} d\phi\, \cos[\phi/2] = 2/\pi \tag{A3}$$

For simplicity the factor $|\cos[\phi/2]|$ is replaced by $2/\pi$ in the sequel. Then, averaging over the four possible states at each bend yields

$$\begin{aligned}\langle\beta_m\rangle &= \left(\frac{1}{(K+1)^2}\right)\cdot 0 + \frac{2(K/(K+1)^2)m\theta_1}{2} \\ &\quad + \left(\frac{K^2}{(K+1)^2}\right)\frac{(2/\pi)m\theta_1}{2} \\ &= m\theta_1(K + 2K^2/\pi)/(K+1)^2\end{aligned} \tag{A4}$$

and

$$\begin{aligned}&\langle\cos[\beta_m - \langle\beta_m\rangle]\rangle \\ &= (1/(K+1))^2\left\{\cos\left[\frac{m\theta_1(K+2K^2/\pi)}{(K+1)^2}\right]\right. \\ &\quad + 2K\cos\left[m\theta_1\left(0.5 - \frac{K+2K^2/\pi}{(K+1)^2}\right)\right] \\ &\quad \left. + K^2\cos\left[m\theta_1\left(\frac{2}{\pi} - \frac{K+2K^2/\pi}{(K+1)^2}\right)\right]\right\}\end{aligned} \tag{A5}$$

Inserting Eqs. A2 and A5 into A1 yields

$$\begin{aligned}P_{sr} &= \left\{\frac{mh}{K+1} + \left(\frac{K}{K+1}\right)\left(\frac{h}{\theta_1}\right)2\left|\sin\left[\frac{m\theta_1}{2}\right]\right|\right\} \\ &\quad \div\left\{1 - (1/(K+1))^2\left(\cos\left[\frac{m\theta_1(K+2K^2/\pi)}{(K+1)^2}\right]\right.\right. \\ &\quad + 2K\cos\left[m\theta_1\left(0.5 - \frac{K+2K^2/\pi}{(K+1)^2}\right)\right] \\ &\quad \left.\left. + K^2\cos\left[m\theta_1\left(\frac{2}{\pi} - \frac{K+2K^2/\pi}{(K+1)^2}\right)\right]\right)\right\}\end{aligned} \tag{A6}$$

APPENDIX B

Distribution of τ_R values

A rough estimate of the distribution of τ_R is obtained by making the following assumptions, which though not strictly valid, may be reasonable approximations on average. When the different kinds of bends are applied in succession, 1) the common permanent bend reduces the end-to-end distance of the rod slightly from L to l_{pb} by the factor l_{pb}/L; 2) any given slowly relaxing bend further slightly reduces the end-to-end distance to $l_{pb,sr}$ by the *ratio* $l_{pb,sr}/l_{pb} = l_{sr}/L$, which is the same as if that slowly relaxing bend were applied directly to a rigid rod of length L to yield l_{sr}; 3) any given dynamic bend acting on an intrinsically curved filament with end-to-end distance $l_{pb,sr}$ further slightly reduces the end-to-end distance to $l_{pb,sr,d}$ by the ratio $l_{pb,sr,d}/l_{pb,sr} = l_d/L$, which is the same as if that dynamic bend had been applied directly to rod of length L to yield l_d. For a molecule with the common permanent bend and a given slowly relaxing bend, it is assumed that the end-over-end tumbling time is given approximately by $\tau_R \propto \langle l^3_{pb,sr,d}\rangle_d$, wherein the averaging is taken *only over the dynamic bends*. Making use of the relations assumed above yields

$$\tau_R \propto (l_{sr}/L)^3(l_{pb}/L)^3\langle l_d^3/L^3\rangle_d L^3 \tag{B1}$$

By numerical comparison with the results of Hagerman and Zimm (1981), we have confirmed that $\langle l_d^3/L^3\rangle_d$ is roughly equal to $R_c = \tau_R(wc)/\tau_R(\text{rod})$, where $\tau_R(wc)$ is the tumbling time computed for a wormlike coil with no intrinsic curvature, and $\tau_R(\text{rod})$ is that computed for the straight rigid rod, when $L/P_d \le 1.36$. In Eq. B1 the effect of both dynamic bends and the common permanent bend is to reduce τ_R by the same factor for all molecules. Equation B1 can be written as $\tau_R/\tau_R^o \propto (l_{sr}/L)^3$, where $\tau_R^o \propto \langle l_{pb}^3/L^3\rangle\langle l_d^3/L^3\rangle_d\, L^3$ is the same for all molecules. Hence, the probability distribution of relative τ_R values is the same as the probability distribution of relative l_{sr}^3. The probability distribution $P(l_{sr})$, is taken to be that of a wormlike chain (without intrinsic curvature) with contour length $L = 680$ Å and persistence length $P_{sr} = 1500$ Å. That is the approximate value reckoned from Eq. 3 by using $P_{tot} = 500$ Å, $P_{pb} = 1370$ Å, and $P_d = 1700$ Å, and will prove to be approximately self-consistent, in the sense that the final estimate, $P_{sr} = 1300$ Å, is not very different. The protocol for simulating chain configurations, which uses von Neumann's method for modeling a continuous random variable (Sobol', 1994), is described elsewhere (Schurr and Fujimoto, submitted for publication). The simulated distribution is divided into fifths of the total population. The uppermost fifth spans a range of end-to-end distances from $l_{sr} = L$ down to about the l_{sr} value corresponding to the maximum in $P(l_{sr})$. The measured τ_R of the terminal relaxation process in $S(t)$ is identified with τ_{R1} of this uppermost fifth of the population, so we set $\tau_{R1} = \tau_R$. It is then assumed that for each other fifth ($j = 2, \ldots 5$) of the population, $\tau_{Rj}/\tau_{R1} = \langle l_{sr}^3\rangle_j/\langle l_{sr}^3\rangle_1$, where $\langle l_{sr}^3\rangle_j$ is the mean cubed end-to-end distance for the jth subset of the total population. In this way the total population is subdivided into five components, each with its appropriately scaled τ_{Rj}. The $F_n(t)$ functions in Eq.

7 are reckoned separately for each fifth of the population by using the appropriate $D_{Rj} = 1/6\tau_{Rj}$, and averaged together.

This work was supported in part by National Science Foundation Grant MCB 9607344.

REFERENCES

Allison, S. A. 1983. Torsion dynamics in linear macromolecules: exact inclusion of hydrodynamic interaction. *Macromolecules.* 16:421–425.

Allison, S., R. Austin, and M. Hogan. 1989. Bending and twisting dynamics of short linear DNAs. Analysis of the triplet anisotropy decay of a 209 base pair fragment by Brownian simulation. *J. Chem. Phys.* 90: 3843–3854.

Allison, S. A., and P. Nambi. 1992. Electric dichroism and birefringence decay of short DNA restriction fragments studied by Brownian dynamics simulation. *Macromolecules.* 25:759–768.

Allison, S. A., and J. M. Schurr. 1979. Torsion dynamics and depolarization of fluorescence of linear macromolecules. I. Theory and application to DNA. *Chem. Phys.* 41:35–59.

Allison, S. A., and J. M. Schurr. 1997. Effect of regular anisotropic permanent bending on the diffusional spinning and fluorescence polarization anisotropy of short DNA fragments studied by Brownian dynamics simulation. *Macromolecules.* 30:7131–7142.

Bergmann, K., and C. T. O'Konski. 1963. A spectroscopic study of methylene blue monomer, dimer, and complexes with montmorillonte. *J. Phys. Chem.* 67:2169–2180.

Bolshoy, A., P. McNamara, R. E. Harrington, and E. N. Trifonov. 1991. Curved DNA without A-A: experimental estimation of all 16 DNA wedge angles. *Proc. Natl. Acad. Sci. USA.* 88:2312–2316.

Brukner, I., S. Susic, M. Dlakic, A. Savic, and S. Pongor. 1994. Physiological concentration of magnesium ions induces a strong macroscopic curvature in GGGCCC-containing DNA. *J. Mol. Biol.* 236:26–32.

Chan, S. S., K. J. Breslauer, M. E. Hogan, D. J. Kessler, R. H. Austin, J. Ojemann, J. M. Passner, and N. C. Wiles. 1990. Physical studies of DNA premelting equilibria in duplexes with and without homo dA · dT tracts: correlations with DNA bending. *Biochemistry.* 29:6161–6171.

Chirico, G., and J. Langowski. 1994. Kinetics of DNA supercoiling studied by Brownian dynamics simulation. *Biopolymers.* 34:415–433.

Clendenning, J. B., and J. M. Schurr. 1994. Circularization of small DNAs in the presence of ethidium: a theoretical analysis. *Biopolymers.* 34: 849–868.

Davis, N. A., S. S. Majee, and J. D. Kahn. 1999. TATA box DNA deformation with and without the TATA box-binding protein. *J. Mol. Biol.* 29:249–265.

Delrow, J. J., P. J. Heath, and J. M. Schurr. 1997. On the origin of the temperature dependence of the supercoiling free energy. *Biophys. J.* 73:2688–2701.

Diebold, R. J., N. Rajaram, D. A. Leonard, and T. K. Kerppola. 1998. Molecular basis of cooperative DNA bending and oriented heterodimer binding in the NFAT1-Fos-Jun-ARRE2 complex. *Proc. Natl. Acad. Sci. USA.* 95:7915–7920.

Diekmann, S. 1987. Temperature and salt dependence of the gel migration anomaly of curved DNA fragments. *Nucleic Acids Res.* 15:247–265.

Diekmann, S., W. Hillen, B. Morgeneyer, R. D. Wells, and D. Pörschke. 1982. Orientation relaxation of DNA restriction fragments and the internal mobility of the double helix. *Biophys. Chem.* 15:263–270.

Dlakic, M., and R. E. Harrington. 1995. Bending and torsional flexibility of G/C-rich sequences as determined by cyclization assays. *J. Biol. Chem.* 270:29945–29952.

Dlakic, M., and R. E. Harrington. 1996. The effects of sequence context on DNA curvature. *Proc. Natl. Acad. Sci. USA.* 93:3847–3852. [published erratum appears in *Proc. Natl. Acad. Sci. USA.* 1996 Aug 6;93(16): 8796].

Dlakic, M., and R. E. Harrington. 1998. Unconventional helical phasing of repetitive DNA motifs reveals their relative bending contributions. *Nucleic Acids Res.* 26:4274–4279.

Eden, D., and C. Sunshine. 1989. Transient electric birefringence studies of bending thermodynamics and internal bending dynamics of short DNA restriction fragments. *In* Dynamic Behavior of Macromolecules, Colloids, Liquid Crystals and Biological Systems by Optical and Electrooptical Methods. H. Watanabe, editor. Hirokawa, Tokyo.

Elias, J. G., and D. Eden. 1981. Transient electric birefringence study of the persistence length and electrical polarizability of restriction fragments of DNA. *Macromolecules.* 14:410–419.

Elvingson, C. 1992. Computer simulation of the structure of DNA molecules in an electric field. *Biophys. Chem.* 43:9–19.

Engelhorn, M., and J. Geiselmann. 1998. Maximal transcription activation by the IHF protein of *Escherichia coli* depends on optimal DNA bending by the activator. *Mol. Microbiol.* 30:431–441.

Frank-Kamenetskii, M. D., A. V. Lukashin, V. V. Anshelevich, and A. V. Vologodskii. 1985. Torsional and bending rigidity of the double helix from data on small DNA rings. *J. Biomol. Struct. Dyn.* 2:1005–1012.

Fujimoto, B. S., J. B. Clendenning, J. J. Delrow, P. J. Heath, and J. M. Schurr. 1994a. Fluorescence and photobleaching studies of methylene blue binding to DNA. *J. Phys. Chem.* 98:6633–6643.

Fujimoto, B. S., J. M. Miller, N. S. Ribeiro, and J. M. Schurr. 1993. Rotational dynamics of short DNAs. *Proc. SPIE-Int. Soc. Opt. Eng.* 1922:360–367.

Fujimoto, B. S., J. M. Miller, N. S. Ribeiro, and J. M. Schurr. 1994b. Effects of different cations on the hydrodynamic radius of DNA. *Biophys. J.* 67:304–308.

Fujimoto, B. S., and J. M. Schurr. 1990. Dependence of the torsional rigidity of DNA on base composition. *Nature.* 344:175–177.

Gaudin, F., L. Chanteloupe, N. T. Thuong, and G. Lancelot. 1997. Selectively ^{13}C-enriched DNA: dynamics of the C1′H1′ and C5′H1′ C5′H5′ vectors in d(CGCAAATTTCCG)$_2$. *Magn. Reson. Chem.* 35:561–565.

Gaudin, F., F. Paquet, L. Chanteloup, J.-M. Beau, N. T. Thuong, and G. Lancelot. 1995. Selectively ^{13}C-enriched DNA: dynamics of the C1′H1′ vector in d(CGCAAATTTGCG)$_2$. *J. Biomol. NMR.* 5:49–58.

Gebe, J. A., S. A. Allison, J. B. Clendenning, and J. M. Schurr. 1995. Monte Carlo simulations of supercoiling free energies for unknotted and trefoil knotted DNAs. *Biophys. J.* 68:619–633.

Gebe, J. A., J. J. Delrow, P. J. Heath, B. S. Fujimoto, D. W. Stewart, and J. M. Schurr. 1996. Effects of Na^+ and Mg^{2+} on the structures of supercoiled DNAs: comparison of simulations with experiments. *J. Mol. Biol.* 262:105–128.

Geiselmann, J. 1997. The role of DNA conformation in transcriptional initiation and activation in *Escherichia coli. Biol. Chem.* 378:599–607.

Gralla, J. D. 1991. Transcriptional control—lessons from an *E. coli* promoter data base. *Cell.* 66:415–418.

Gralla, J. D. 1996. Activation and repression of *E. coli* promoters. *Curr. Opin. Genet. Dev.* 6:526–530.

Grosschedl, R., K. Giese, and J. Pagel. 1994. HMG domain proteins: architectural elements in the assembly of nucleoprotein structures. *Trends Genet.* 10:94–100.

Hagerman, P. J. 1981. Investigation of the flexibility of DNA using transient electric birefringence. *Biopolymers.* 20:1503–1535.

Hagerman, P. J. 1988. Flexibility of DNA. *Annu. Rev. Biophys. Biophys. Chem.* 17:265–286.

Hagerman, P. J., and V. A. Ramadevi. 1990. Application of the method of phage T4-catalyzed ring-closure to the study of DNA structure. I. Computational analysis. *J. Mol. Biol.* 212:351–362.

Hagerman, P. J., and B. H. Zimm. 1981. Monte Carlo approach to the analysis of the rotational diffusion of wormlike chains. *Biopolymers.* 20:1481–1502.

Hagmar, P., S. Pierrou, P. Nielsen, B. Norden, and M. Kubista. 1992. Ionic strength dependence of the binding of methylene blue to chromatin and calf thymus DNA. *J. Biomol. Struct. Dyn.* 9:667–679.

Harrington, R. E. 1993. Studies of DNA bending and flexibility using gel electrophoresis. *Electrophoresis.* 14:732–746.

Heath, P. J., S. A. Allison, J. A. Gebe, and J. M. Schurr. 1995. A theory for electric dichroism and birefringence decays and depolarized dynamic light scattering of weakly bending rods. *Macromolecules*. 28: 6600–6607.

Heath, P. J., J. B. Clendenning, B. S. Fujimoto, and J. M. Schurr. 1996a. Effect of bending strain on the torsion elastic constant of DNA. *J. Mol. Biol.* 260:718–730.

Heath, P. J., J. A. Gebe, S. A. Allison, and J. M. Schurr. 1996b. Comparison of analytical theory with Brownian dynamics simulations for small linear and circular DNAs. *Macromolecules.* 29:3583–3596.

Hodges-Garcia, Y., and P. J. Hagerman. 1995. Investigation of the influence of cytosine methylation on DNA flexibility. *J. Biol. Chem.* 270: 197–201.

Hogan, M., J. LeGrange, and B. Austin. 1983. Dependence of DNA helix flexibility on base composition. *Nature (Lond.).* 304:752–754.

Hogan, M., J. Wang, R. H. Austin, C. L. Monitto, and S. Hershkowitz. 1982. Molecular motion of DNA as measured by triplet anisotropy decay. *Proc. Natl. Acad. Sci. USA.* 79:3518–3522.

Horowitz, D. S., and J. C. Wang. 1984. Torsional rigidity of DNA and length dependence of the free energy of DNA supercoiling. *J. Mol. Biol.* 173:75–91.

Hustedt, E. J., A. Spaltenstein, J. J. Kirchner, P. B. Hopkins, and B. H. Robinson. 1993. Motions of short DNA duplexes: an analysis of DNA dynamics using an EPR-active probe. *Biochemistry.* 32:1774–1787.

Ikeda, K., K. Nagano, and K. Kawakami. 1993. Possible implications of Sp1-induced bending of DNA on synergistic activation of transcription. *Gene.* 136:341–343.

Kahn, J. D., and D. M. Crothers. 1998. Measurement of the DNA bend angle induced by the catabolite activator protein using Monte Carlo simulation of cyclization kinetics. *J. Mol. Biol.* 276:287–309.

Kennedy, M. A., S. T. Nuutero, J. T. Davis, G. Drobny, and B. R. Reid. 1993. Mobility at the TpA cleavage in the T_3A_3-containing AhaIII and PmeI restriction sequences. *Biochemistry.* 32:8022–8035.

Kim, J. L., and S. K. Burley. 1994. 1.9 Å resolution refined structure of TBP recognizing the minor groove of TATAAAAG. *Nat. Struct. Biol.* 1:638–653.

Kolb, A., A. Spassky, C. Chapon, B. Blazy, and H. Buc. 1983. On the different binding affinities of CRP at the lac, gal and malT promoter regions. *Nucleic Acids Res.* 11:7833–7852.

Liu-Johnson, H. N., M. R. Gartenberg, and D. M. Crothers. 1986. The DNA binding domain and bending angle of *E. coli* CAP protein. *Cell.* 47:995–1005.

McAteer, K., P. D. Ellis, and M. A. Kennedy. 1995. The effects of sequence context on base dynamics at TpA steps in DNA studied by NMR. *Nucleic Acids Res.* 23:3962–3966.

Mossing, M. C., and M. T. Record, Jr. 1986. Upstream operators enhance repression of the lac promoter. *Science.* 233:889–892.

Naimushin, A. N. 1999. A Transient Polarization Grating Method to Study Tumbling and Bending Dynamics of DNA. Ph.D. Dissertation; University of Washington, Seattle.

Naimushin, A. N., B. S. Fujimoto, and J. M. Schurr. 1999a. Effect of intermolecular electrostatic interactions on the end-over-end rotational dynamics of 200-base-pair DNAs. *Macromolecules*. 32:8210–8219.

Naimushin, A. N., B. S. Fujimoto, and J. M. Schurr. 1999b. A transient polarization grating method to study tumbling and bending dynamics of DNA. *Rev. Sci. Instrum.* 70:2471–2480.

Nelson, H. C., J. T. Finch, B. F. Luisi, and A. Klug. 1987. The structure of an oligo(dA) · oligo(dT) tract and its biological implications. *Nature.* 330:221–226.

Nordén, B., and F. Tjerneld. 1982. Structure of methylene blue-DNA complexes studied by linear and circular dichroism spectroscopy. *Biopolymers.* 21:1713–1734.

Okonogi, T. M., A. Reese, S. C. Alley, P. B. Hopkins, and B. H. Robinson. 1999. Flexibility of duplex DNA on the sub-microsecond timescale. *Biophys. J.* 77:3256–3276.

Paquet, F., F. Gaudin, and G. Lancelot. 1996. Selectively ^{13}C-enriched DNA: evidence from $^{13}C1'$ relaxation rate measurements of an internal dynamics sequence effect in the *lac* operator. *J. Biomol. NMR.* 8:252–260.

Parkhurst, K. M., M. Brenowitz, and L. J. Parkhurst. 1996. Simultaneous binding and bending of promoter DNA by the TATA binding protein: real time kinetic measurements. *Biochemistry.* 35:7459–7465.

Parkhurst, K. M., R. M. Richards, M. Brenowitz, and L. J. Parkhurst. 1999. Intermediate species possessing bent DNA are present along the pathway to formation of a final TBP-TATA complex. *J. Mol. Biol.* 289: 1327–1341.

Passner, J. M., and T. A. Steitz. 1997. The structure of a CAP-DNA complex having two cAMP molecules bound to each monomer. *Proc. Natl. Acad. Sci. USA.* 94:2843–2847.

Perez-Martin, J., and V. de Lorenzo. 1997. Clues and consequences of DNA bending in transcription. *Annu. Rev. Microbiol.* 51:593–628.

Pörschke, D. 1991. Persistence length and bending dynamics of DNA from electrooptical measurements at high salt concentrations. *Biophys. Chem.* 40:169–179.

Pörschke, D., W. Zacharias, and R. D. Wells. 1987. B-Z DNA junctions are neither highly flexible nor strongly bent. *Biopolymers.* 26:1971–1974.

Rice, P. A., S. Yang, K. Mizuuchi, and N. A. Nash. 1996. Crystal structure of an IHF-DNA complex: a protein-induced DNA U-turn. *Cell.* 87: 1295–1306.

Rippe, K., P. H. von Hippel, and J. Langowski. 1995. Action at a distance: DNA-looping and initiation of transcription. *Trends Biochem. Sci.* 20: 500–506.

Schellman, J. A., and S. C. Harvey. 1995. Static contributions to the persistence length of DNA and dynamic contributions to DNA curvature. *Biophys. Chem.* 55:95–114.

Schleif, R. 1992. DNA looping. *Annu. Rev. Biochem.* 61:199–223.

Schultz, S. C., G. C. Shields, and T. A. Steitz. 1991. Crystal structure of a CAP-DNA complex: the DNA is bent by 90 degrees. *Science.* 253: 1001–1007.

Schurr, J. M. 1984. Rotational diffusion of deformable macromolecules with mean local cylindrical symmetry. *Chem. Phys.* 84:71–96.

Schurr, J. M. 1985. Effect of anisotropic bending rigidity and finite twisting rigidity on statistical properties of DNA model filaments. *Biopolymers.* 24:1233–1246.

Schurr, J. M., H. P. Babcock, and J. A. Gebe. 1995. Effect of anisotropy of the bending rigidity on the supercoiling free energy of small circular DNAs. *Biopolymers.* 36:633–641.

Schurr, J. M., J. J. Delrow, B. S. Fujimoto, and A. S. Benight. 1997a. The question of long-range allosteric transitions in DNA. *Biopolymers.* 44: 283–308.

Schurr, J. M., and B. S. Fujimoto. 1988. The amplitude of local angular motions of intercalated dyes and bases in DNA. *Biopolymers.* 27: 1543–1569.

Schurr, J. M., B. S. Fujimoto, A. Reese, and B. H. Robinson. 1997b. Comment on "Diffusional spinning as a probe of DNA fragments conformation" [*J. Chem. Phys.* 104:6058 (1996)]. *J. Chem. Phys.* 106: 815–816.

Schurr, J. M., B. S. Fujimoto, P. Wu, and L. Song. 1992. Fluorescence studies of nucleic acids. Dynamics, rigidities, and structures. *In* Topics in Fluorescence Spectroscopy. Lakowicz, editor. Plenum Press, New York. 137–229.

Shimada, J., and H. Yamakawa. 1984. Ring closure probabilities for twisted wormlike chains. Application to DNA. *Macromolecules.* 17: 689–698.

Shimada, J., and H. Yamakawa. 1985. Statistical mechanics of DNA topoisomers. The helical wormlike chain. *J. Mol. Biol.* 184:319–329.

Shore, D., and R. L. Baldwin. 1983. Energetics of DNA twisting. II. Topoisomer analysis. *J. Mol. Biol.* 170:983–1007.

Sjottem, E., C. Andersen, and T. Johansen. 1997. Structural and functional analyses of DNA bending induced by Sp1 family transcription factors. *J. Mol. Biol.* 267:490–504.

Sobol', I. M. 1994. A Primer for the Monte Carlo Method. CRC Press, Ann Arbor, MI. 30.

Song, L., S. A. Allison, and J. M. Schurr. 1990. Normal mode theory for the Brownian dynamics of a weakly bending rod: comparison with Brownian dynamics simulations. *Biopolymers.* 29:1773–1791.

Song, L., and J. M. Schurr. 1990. Dynamic bending rigidity of DNA. *Biopolymers.* 30:229–237.

Spielmann, H. P. 1998. Dynamics in psoralen-damaged DNA by ^{1}H-detected natural abundance ^{13}C NMR spectroscopy. *Biochemistry.* 37: 5426–5438.

Sprous, D., W. Zacharias, Z. A. Wood, and S. C. Harvey. 1995. Dehydrating agents sharply reduce curvature in DNAs containing A tracts. *Nucleic Acids Res.* 23:1816–1821.

Stellwagen, N. C. 1983. Anomalous electrophoresis of deoxyribonucleic acid restriction fragments on polyacrylamide gels. *Biochemistry.* 22: 6186–6193.

Taylor, W. H., and P. J. Hagerman. 1990. Application of the method of phage T4 DNA ligase-catalyzed ring-closure to the study of DNA structure. II. NaCl-dependence of DNA flexibility and helical repeat. *J. Mol. Biol.* 212:363–376.

Tirado, M. M., and J. Garcia de la Torre. 1979. Translational friction coefficients of rigid symmetric top macromolecules. Application to circular cylinders. *J. Chem. Phys.* 71:2581–2587.

Tirado, M. M., and J. Garcia de la Torre. 1980. Rotational dynamics of rigid symmetric top macromolecules. Application to circular cylinders. *J. Chem. Phys.* 73:1986–1993.

Trifonov, E. N., R. K.-Z. Tan, and S. C. Harvey. 1987. Static persistence length of DNA. *In* DNA Bending and Curvature. W. K. Olson, M. H. Sarma, and M. Sundaralingam, editors. Adenine Press, Schenectady, NY. 243–254.

von Jena, A., and H. E. Lessing. 1979. Theory of laser-induced amplitude and phase gratings including photoselection, orientational relaxation and population kinetics. *Optical and Quantum Electronics.* 11:419–439.

Wang, M. D., H. Yin, R. Landick, J. Gelles, and S. M. Block. 1997. Stretching DNA with optical tweezers. *Biophys. J.* 72:1335–1346.

Wu, H. M., and D. M. Crothers. 1984. The locus of sequence-directed and protein-induced DNA bending. *Nature.* 308:509–513.